© 2015. Published by The Company of Biologists Ltd | Journal of Cell Science (2015) 128, 1453 doi:10.1242/jcs.170944

CORRECTION

Cooperative functions of the two F-BAR proteins Cip4 and Nostrin in the regulation of E-cadherin in epithelial morphogenesis

Thomas Zobel, Klaus Brinkmann, Nicole Koch, Katharina Schneider, Eric Seemann, Astrid Fleige, Britta Qualmann, Michael M. Kessels and Sven Bogdan

There was an error published in *J. Cell Sci.* **128**, 499–515.

On p. 507 of this article, the legend of Fig. 6 contained an incomplete description of panel B.

The correct sentence should read:

(B) Wild type stage 4 egg chamber stained for Armadillo and E-cadherin; arrowhead indicates apical E-cadherin localization in follicle cells.

We apologise to the readers for any confusion that this error might have caused.

© 2015. Published by The Company of Biologists Ltd | Journal of Cell Science (2015) 128, 499–515 doi:10.1242/jcs.155929

RESEARCH ARTICLE

Cooperative functions of the two F-BAR proteins Cip4 and Nostrin in the regulation of E-cadherin in epithelial morphogenesis

Thomas Zobel[1,*], Klaus Brinkmann[1,*], Nicole Koch[2], Katharina Schneider[2], Eric Seemann[3], Astrid Fleige[1], Britta Qualmann[2], Michael M. Kessels[2] and Sven Bogdan[1,‡]

ABSTRACT

F-BAR proteins are prime candidates to regulate membrane curvature and dynamics during different developmental processes. Here, we analyzed *nostrin*, a so-far-unknown *Drosophila melanogaster* F-BAR protein related to Cip4. Genetic analyses revealed a strong synergism between *nostrin* and *cip4* functions. Whereas single mutant flies are viable and fertile, combined loss of *nostrin* and *cip4* results in reduced viability and fertility. Double mutant escaper flies show enhanced wing polarization defects and females exhibit strong egg chamber encapsulation defects. Live-imaging analysis suggests that the observed phenotypes are caused by an impaired turnover of E-cadherin at the membrane. Simultaneous knockdown of Cip4 and Nostrin strongly increases the formation of tubular E-cadherin vesicles at adherens junctions. Cip4 and Nostrin localize at distinct membrane subdomains. Both proteins prefer similar membrane curvatures but seem to form distinct membrane coats and do not heterooligomerize. Our data suggest an important synergistic function of both F-BAR proteins in membrane dynamics. We propose a cooperative recruitment model, in which Cip4 initially promotes membrane invagination and early-actin-based endosomal motility, and Nostrin makes contacts with microtubules through the kinesin Khc-73 for trafficking of recycling endosomes.

KEY WORDS: F-BAR proteins, Cip4, Toca-1, Nostrin, E-cadherin, Membrane trafficking, *Drosophila*, Cell polarity, Wing epithelium, Oogenesis, Kinesins, Microtubules

INTRODUCTION

Members of the Fes–CIP4 homology Bin–amphiphysin–Rvs161/167 (F-BAR) protein family form crescent-shaped dimers that are able to shape membranes into vesicles and tubules (McMahon and Gallop, 2005; Fütterer and Machesky, 2007; Heath and Insall, 2008; Koch et al., 2012b; Qualmann et al., 2011; Suetsugu, 2010; Suetsugu and Gautreau, 2012). F-BAR proteins have been grouped into six subfamilies, the Cdc42-interacting protein 4 (Cip4) subfamily, the Fes subfamily of non-receptor tyrosine kinases, the protein kinase C and casein kinase substrate in neurons protein (pacsin) subfamily, the Slit–Robo RhoGTPase-activating proteins (SrGAPs), the FCH-domain-only (FCHO) and the proline-serine-threonine phosphatase-interacting protein (PSTPIP) subfamilies (Ahmed et al., 2010; Heath and Insall, 2008). The phylogenetic subgrouping is mainly based on structural similarities of the N-terminal F-BAR module, and on the composition and architecture of C-terminal domains. Distinct differences of the intrinsic F-BAR domain curvature observed among the different F-BAR-domain proteins are thought to reflect characteristic preferences in sensing and/or inducing membrane invaginations of different curved geometry. Consistent with this idea, members of FCHO subfamily bind to very low membrane curvatures and are found to be essential for the initial step of membrane invagination in endocytosis (Henne et al., 2010). Other F-BAR proteins, such as members of the Cip4 subfamily, which includes the Cdc42-interacting protein 4 (Cip4), the transducer of Cdc42-dependent actin assembly (Toca-1) and the formin-binding protein 17 (FBP17), have a preference for higher membrane curvatures present in later steps during vesicle formation (Frost et al., 2008; Frost et al., 2009; Shimada et al., 2007).

Unlike those of the FCHO subfamily, Cip4 subfamily proteins contain a C-terminal SH3 domain that binds dynamin and factors that promote actin filament formation (Itoh and De Camilli, 2006; Tsujita et al., 2006). All three members of the Cip4 subfamily are able to activate N-WASP by promoting Arp2/3-mediated actin nucleation *in vitro* (Ho et al., 2004). Cip4 and Toca-1 also associate with Cdc42 through a central coiled-coil region (Aspenström, 2009). The current view is that Cip4-related proteins may stabilize plasma membrane invaginations and, subsequently, recruit dynamin and WASP proteins to the neck of endocytic pits that mediate the constriction and scission of vesicles. Recruitment of WASP proteins to newly formed vesicles also promotes the formation of actin comet tails that provide the driving force for endocytic vesicle movement (Bu et al., 2010; Fricke et al., 2009). However, our understanding of how F-BAR proteins function *in vivo* in a physiological context is still incomplete because loss-of-function studies in higher organisms are limited. Mice that lack Cip4 are viable and show only a weak endocytosis defect of the insulin-responsive glucose transporter Glut4 (Feng et al., 2010). Mutant animals also display a reduced platelet production and defective integrin-dependent T-cell adhesion, both defects are probably caused by decreased WASP-dependent actin polymerization, rather than impaired endocytosis (Chen et al., 2013). Given the mild phenotypes, the two other Cip4-like subfamily members Toca-1 and FBP17 might have redundant functions and could compensate for the loss of Cip4 function.

Initial RNA interference (RNAi) studies in *Drosophila melanogaster* revealed that Cip4 regulates dynamin-dependent endocytosis of E-cadherin at adherens junctions (Leibfried et al., 2008). As in mammals, function of *cip4* is not essential for fly development (Fricke et al., 2009). *cip4* mutants show duplicated

[1]Institute for Neurobiology, University of Münster, Münster 48149, Germany. [2]Institute of Biochemistry I, Jena University Hospital – Friedrich Schiller University Jena, 07743 Jena, Germany. [3]Institute of Biochemistry I and Electron Microscopy Center, Jena University Hospital – Friedrich Schiller University Jena, 07743 Jena, Germany.
*These authors contributed equally to this work

‡Author for correspondence (sbogdan@uni-muenster.de)

Received 1 May 2014; Accepted 6 November 2014

Journal of Cell Science (2015) 128, 499–515 doi:10.1242/jcs.155929

wing hairs because of an impaired endocytosis. Further analyses revealed that Cip4 acts downstream of Cdc42 to activate the WASP–WAVE–Arp2/3 pathway in the notum and the wing epithelium (Leibfried et al., 2008; Fricke et al., 2009). In addition, a postsynaptic, endocytosis-independent function of Cip4 has been identified at the neuromuscular junction. This function also depends on an interaction with the Cdc42–WASP–Arp2/3 pathway but does not require a functional F-BAR domain (Nahm et al., 2010).

The *Drosophila* genome contains an additional, not yet characterized gene encoding a Cip4-like F-BAR protein with highest similarities to human Nostrin (CG42388). Human Nostrin was originally identified as an interaction partner of the endothelial nitric oxide synthase (eNos, Zimmermann et al., 2002). Cell culture studies further suggest that Nostrin regulates N-WASP and/or dynamin-dependent trafficking and the activity of endothelial nitric oxide synthase (eNos) (Icking et al., 2005; Zimmermann et al., 2002). However, an *in vivo* role of Nostrin in the regulation of eNos activity or endocytosis has not yet been found. A recent loss-of-function study in zebrafish and mice revealed a role of Nostrin in endothelial cell morphology during vascular development (Kovacevic et al., 2012). Antisense morpholino oligonucleotide (MO)-mediated knockdown of Nostrin in developing zebrafish affects the migration of endothelial tip cells of intersegmental blood vessels (Kovacevic et al., 2012). Remarkably, *nostrin*-knockout mice are viable and show only mild retinal angiogenesis defects (Kovacevic et al., 2012). This suggests that other F-BAR proteins compensate for *nostrin* function in mutant mice.

As *Drosophila* contains only a single gene copy of each F-BAR subfamily (Fricke et al., 2010), studies in flies are well-suited to address putative functional redundancies within and between F-BAR domain subfamilies. Here, we present a functional analysis of *CG42388*, which encodes the *Drosophila* Nostrin protein, and its physiological relationship to Cip4. Flies that lack Nostrin are viable and fertile. However, loss of both *nostrin* and *cip4* results in reduced viability and fertility. Double mutant flies show a strong multiple wing hair phenotype and females are semi-sterile. Egg chambers of double mutant flies show strong encapsulation defects that are likely to be caused by an impaired membrane turnover of E-cadherin. Cip4 and Nostrin, preferentially, bind similar membrane curvatures but localize at distinct subdomains of membrane structures in cells. Our data suggest an important, non-redundant function of Cip4 and Nostrin in the regulation of membrane dynamics in epithelial morphogenesis.

RESULTS

Drosophila CG42388 encodes an F-BAR protein with highest similarity to Nostrins

Our previous analysis of cip4/toca-1 (known as *Cip4*, CG15015) in *Drosophila* revealed only a subtle mutant phenotype. In a database search we identified the gene *CG42388* encoding a putative Cip4-like F-BAR protein in *Drosophila* (Fig. 1A). *CG42388* encodes a member of the Nostrin subfamily of F-BAR proteins (Icking et al., 2005; Zimmermann et al., 2002). Nostrins are evolutionarily highly conserved throughout eukaryotes (Fig. 1B). The *Drosophila* gene *CG42388* was therefore termed *nostrin*. It encodes six different isoforms that only differ in their N-terminal sequences (according to Flybase). All isoforms contain an F-BAR and a C-terminal Src-homology 3 (SH3) domain. The largest isoform contains an additional N-terminal exon (exon 1L, see Fig. 1D) encoding about 600 amino acids N-terminally to the F-BAR domain and has no similarities to known proteins. The short isoform (Nostrin short) shares the highest similarity to human NOSTRIN (60% similarity; 26% identity) and displays an N-terminal F-BAR domain as found in most F-BAR proteins (Fig. 1A). Like its human counterpart it also contains an additional coiled-coil domain (position 311–340) predicted by COILS/PCOILS (Lupas, 1996).

Loss-of-*nostrin* mutants are viable and fertile

Recent high-throughput expression data indicate a high expression of Nostrin in ovaries of four day old female flies (Gelbart and Emmert, 2013). Consistently, we found that *nostrin* is maternally provided and during embryonic development the protein is only detectable in total lysates obtained from 0–2 h old embryos (Fig. 1C).

To further analyze the function of *nostrin*, we generated a deletion mutant by using the FRT/FLP system (Golic and Lindquist, 1989; Parks et al., 2004; Fig. 1D). Genomic PCR analysis (data not shown) and western blot analysis confirmed a complete loss of Nostrin protein expression (Fig. 1E). Remarkably, *nostrin* mutant flies are viable and fertile without any obvious phenotypes.

Loss of *nostrin* and *cip4* gene functions results in a reduced viability and fertility, and increased defects of polarization of the wing epithelium

Given the structural similarities between different F-BAR proteins, they might act redundantly *in vivo*; therefore, loss-of-function mutations only result in relatively mild defects. Like *nostrin-null* mutant, flies that lack cip4/toca-1 are viable and fertile (Fricke et al., 2009; Nahm et al., 2010). In contrast to *nostrin* mutants, loss of *cip4* affects wing hair formation (Fricke et al., 2009). Wild type wing cells form a single, distally orientated wing hair, whereas *cip4* mutants frequently show wing hair duplications (Fricke et al., 2009; Fig. 2A,B,I). Interestingly, we found that RNAi leading to simultaneous knockdown of both *cip4* and *nostrin* results in a more-pronounced wing hair phenotype, although suppression of *nostrin* itself alone has no effect on wing hair formation (Fig. 2C–E). Co-suppression of *cip4* and *nostrin* results not only in an increased number of cells with duplicated wing hairs but also induces the formation of multiple wing hairs ($\geq$3 hairs; Fig. 2E). Thus, Cip4 and Nostrin might function synergistically during development.

To further analyze such cooperative function in more detail, we generated double mutant flies that lack both *nostrin* and *cip4* (hereafter referred to as *nost;;cip4* flies). In contrast to single mutants, loss of both these genes results in semi-lethality with strongly reduced number of offspring (only 2.6% of the expected offspring survive to adulthood; supplementary material Fig. S1A). Loss of both *nostrin* and *cip4* results not only in female sterility but also affects the fertility of males (supplementary material Fig. S1B). Additionally, double-mutant escaper flies exhibit wings that comprise a significantly higher number of cells with multiple wing hairs – similar to the phenotype in response to RNAi (Fig. 2F,J). Loss of *nostrin* alone does not affect wing hair formation, whereas overexpression of Nostrin results in a strong multiple wing hair phenotype, as recently found for Cip4 gain-of-function (Fig. 2G,H; Fricke et al., 2009).

Loss of *nostrin* and *cip4* gene functions does not affect Frizzled localization

The formation of a single wing hair depends on the Frizzled planar cell polarity (PCP)-signaling pathway, regulated by a set of

Journal of Cell Science (2015) 128, 499–515 doi:10.1242/jcs.155929

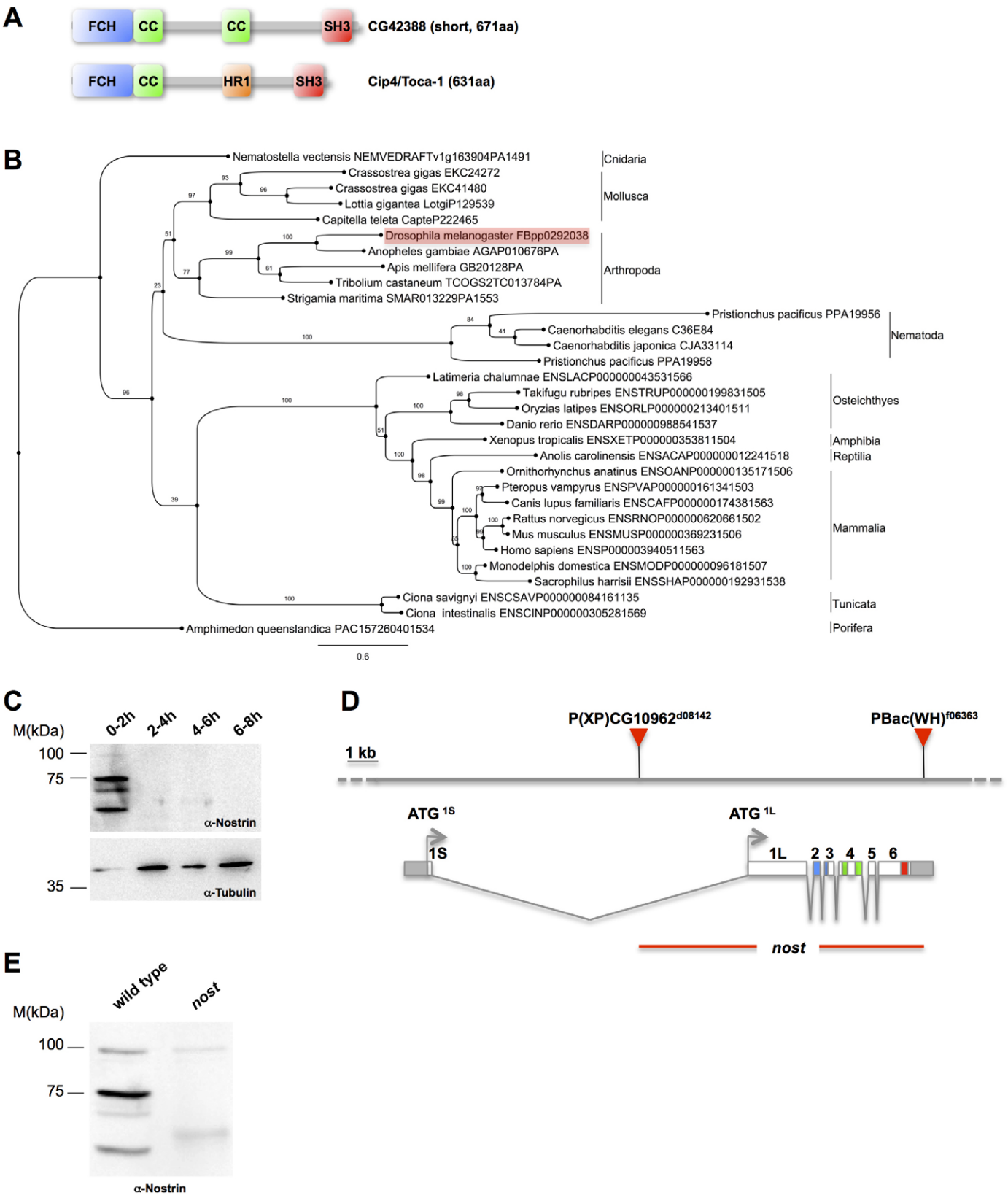

Fig. 1. See next page for legend.

core proteins that define the position and number of emerging wing hairs (Adler, 2012). A key mechanism in the establishment of polarity along the distal–proximal axis is the asymmetric localization of the core PCP proteins, including Frizzled, Flamingo or Van Gogh at the apical surface of the wing cells, shortly before wing hair formation was initiated, ~26–28 h after

Journal of Cell Science (2015) 128, 499–515 doi:10.1242/jcs.155929

Fig. 1. CG42388 encodes a member of the Nostrin subfamily of F-BAR proteins in *Drosophila*. (A) Schematic view of the full-length *Drosophila* CG42388 (Nostrin; short isoform) and Cip4 protein. Like Cip4, Nostrin contains an N-terminal Fer/Cip4 homology (FCH) domain (blue) followed by a coiled-coil (CC) domain (green); together, they are referred to as the F-BAR domain. Nostrin also contains a second coiled-coil domain with weak similarity to the Cdc42-interacting (HR1) domain (orange) of Cip4 and a C-terminal SH3 domain (red). (B) Phylogenetic relationship of Nostrin orthologs. The bootstrap tree values (as a percentage of 100 replicates) are provided at the branches. (C) A polyclonal anti-Nostrin serum only detects Nostrin protein expression in total lysates obtained from 0–2 h-old embryos. The main upper protein band corresponds to the short Nostrin isoform (depicted in A), with an expected molecular mass of about 75 kDa. (D) Schematic overview of the *nostrin* gene locus. *nostrin* is located on the first chromosome. Alternative splicing generates a short (with exon 1S) and a long transcript containing an additional N-terminal exon (1L) that encodes about 600 amino acids in front of the F-BAR domain without any similarities to known proteins. The exons are colored according to the encoding domains (FCH:blue; coiled-coil: green; SH3: red). The precise excision of the two P-element insertions P(XP)CG10962 and PBac{WH}f06363 leads to the deletion of almost all exons. (E) Western blot analysis of wild type and homozygous *nostrin* mutant embryos (staged 0–2 h) confirms the complete loss of Nostrin protein expression.

puparium formation (APF) (Strutt, 2002). Recent studies provide evidence for the involvement of directional transport in the asymmetric accumulation. Frizzled and Flamingo preferentially traffic along apical microtubules, which are aligned along the proximal-distal axis (Shimada et al., 2006). Interestingly, live imaging of pupal wings expressing EGFP-tagged Nostrin (Nostrin–EGFP) revealed a strong accumulation of Nostrin at the apical side of wing cells, as we have recently shown for Cip4 (Fricke et al., 2009; Fig. 2K,L; supplementary material Movie 1). Up to 28 h APF, Nostrin–EGFP vesicles are evenly distributed in the pupal wing (Fig. 2K). Afterwards, Nostrin–EGFP-marked vesicles accumulate at the base of growing prehairs (Fig. 2L–O). Remarkably, Nostrin–EGFP-marked vesicles are transported along microtubules (supplementary material Movies 2 and 9).

To test whether the distribution of the PCP proteins is affected in *nost;;cip4* double mutants, 28 h APF pupal wings were stained with an anti-Frizzled or anti-Flamingo antibody (Fig. 2P–R). However, we found no obvious differences in the *z*-pattern of Frizzled or Flamingo (Fig. 2P,Q; data not shown). In double-mutant cells, Frizzled still accumulates at the distal side as it does in wild type cells. Similar results were obtained with RNAi-mediated double knockdown. Thus, Nostrin and Cip4 might not be involved in the trafficking of PCP core proteins but, rather, affect epithelial packing, a process that requires polarized Rab11-dependent vesicle trafficking of E-cadherin (Classen et al., 2005).

Cell packing is normally remodeled in the wing epithelium shortly before hair formation, which results in hexagonally packed cells (Classen et al., 2005). The hexagonal cell shape, in turn, leads to the formation and distinct orientation of ridges on the adult wing (Doyle et al., 2008). Cuticle refraction microscopy analysis of adult wings reveals that RNAi-mediated knockdown of *cip4* and *nostrin* affects the shape of wing cells, resulting in interrupted ridges (supplementary material Fig. S1C–E). Hence, Nostrin and Cip4 also seem to have an early function in E-cadherin-dependent cell packing.

Cip4 and Nostrin cooperatively act on membrane turnover of E-cadherin at adherens junctions

Previous studies already revealed a role of Cip4 in the regulation of E-cadherin endocytosis (Leibfried et al., 2008). In contrast to *nostrin* knockdown, impaired *cip4* function results in an accumulation of E-cadherin–EGFP-positive vesicular and elongated malformed structures at the cell cortex of the dorsal thorax epithelium (Leibfried et al., 2008; compare Fig. 3A–C, arrowhead in Fig. 3C). Remarkably, simultaneous knockdown of Cip4 and Nostrin significantly increases the formation of tubular E-cadherin vesicles at adherens junctions (Fig. 3D, arrowheads). Such structures were observed very rarely in wild type or *nostrin* deficient tissue (Fig. 3A,B and quantification in Fig. 3E). The junctional surfaces are clearly increased as already observed in *cip4* deficient cells (quantified in Fig. 3F). Time-lapse microscopy further revealed that simultaneous knockdown of Cip4 and Nostrin also affects the stability of adherens junctions (compare supplementary material Movies 3–6). Labeled apical membranes are irregularly shaped and frequently detach between neighboring cells (Fig. 3G, asterisk; supplementary material Movie 6b). Taken together, these data strongly suggest that both F-BAR proteins act together in the regulation of E-cadherin-dependent epithelial morphogenesis.

nost;;cip4 double mutants show strong defects in egg chamber formation resulting from an encapsulation defect

Recent high throughput expression studies revealed a strong expression of Cip4 and Nostrin in the ovary of females (Gelbart and Emmert, 2013). Since *nostrin–cip4* double-mutant (*nost;;cip4*) flies have a strongly reduced number of offspring, we further analyzed double mutant egg chambers for possible morphological defects in more detail. Wild type egg chambers consist of 15 polyploid nurse cells and one oocyte, surrounded by a monolayered epithelium of somatic follicle cells (Fig. 4A). In contrast, approximately half of the *nost;;cip4* double mutant egg chambers show an aberrant number of germline cells (44.8% $n=300$; Fig. 4B,C). Defective egg chambers of stage 9 or older could not be observed. Ovaries of single *nostrin* mutants look wild typic, whereas single *cip4* mutants display similar albeit much weaker defects (12.6% $n=54$; Fig. 4C).

We further analyzed whether the aberrant cell numbers are caused by a defect in the division of the cystoblast or resulted from a defect in the encapsulation of single germline cysts by follicle cells in the germarium. A wild type cystoblast divides four times synchronously with an incomplete cytokinesis. This results in germline cysts with 15 nurse cells and one oocyte that are interconnected by 15 ring canals (Robinson and Cooley, 1997; Fig. 4D). The oocyte originates from one of the first two germline cells and therefore undergoes four divisions resulting in four ring canals. If the cystoblast would divide five times, the resulting egg chambers would consist of 31 nurse cells and an oocyte with five ring canals (supplementary material Fig. S1F–H). In egg chambers with an encapsulation defect, two or more germline cysts would get surrounded by follicle cells as one egg chamber. This would result in 30 nurse cells and two oocytes with four ring canals each (Fig. 4E; supplementary material Fig. S1H). Defective egg chambers of *nost;;cip4* double mutants always exhibit two or more oocytes and the number of ring canals and nurse cells in these egg chambers correlates with the number expected for an encapsulation defect instead of a cytokinesis defect (supplementary material Fig. S1H; Fig. 4E-H). Furthermore, all oocytes in defective egg chambers have four ring canals (Fig. 4F). Whereas oocytes in wild type egg chambers are always localized at the posterior, oocytes in mutant egg chambers are randomly positioned (Fig. 4F, arrows).

Journal of Cell Science (2015) 128, 499–515 doi:10.1242/jcs.155929

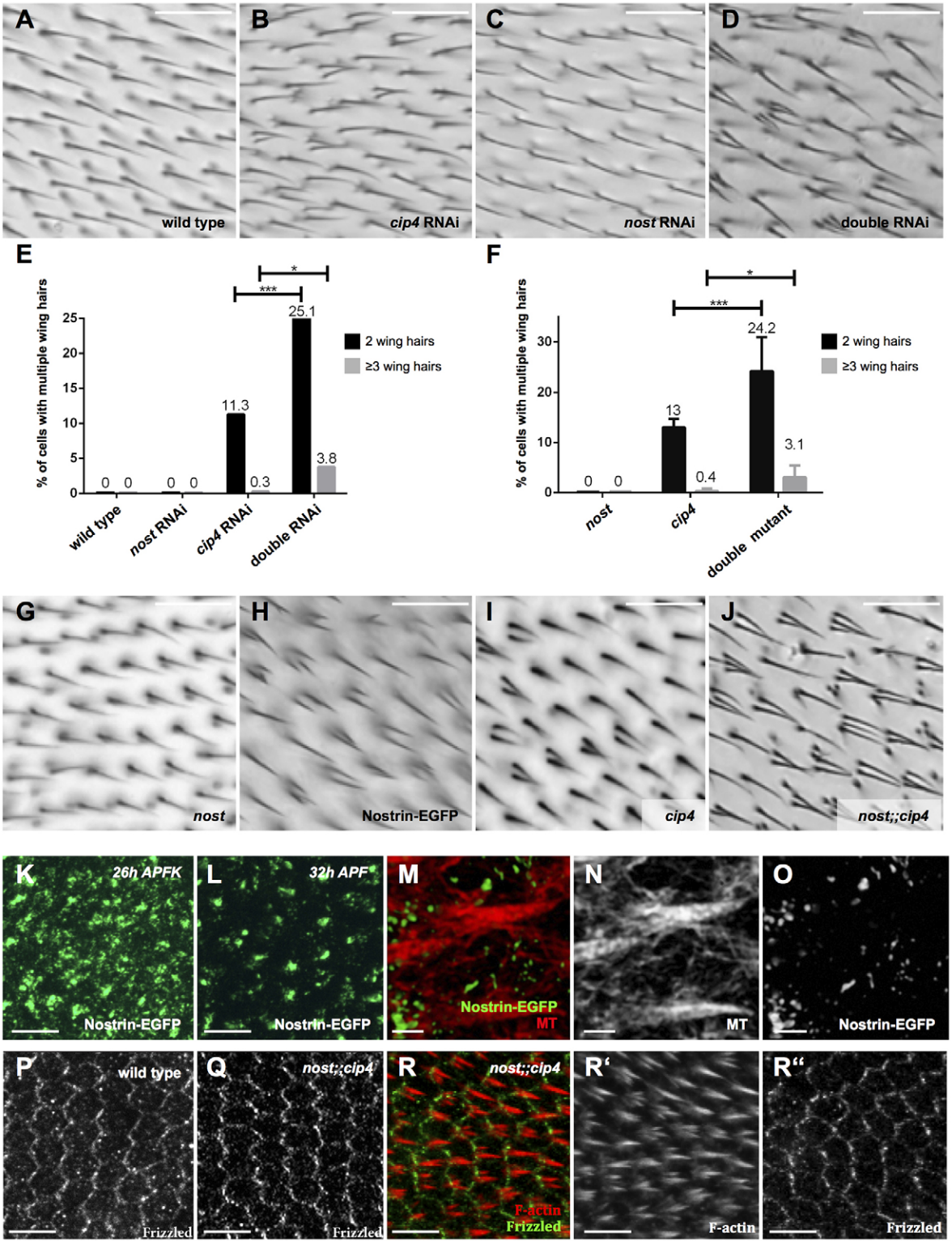

Fig. 2. Loss of *nostrin* and *cip4* gene functions result in an enhanced multiple wing hair phenotype. (A–D,G–J) Magnifications of a defined area of adult female wings expressing the indicated RNAi transgenes in the engrailed expression pattern (A–D) or mutant wings of indicated genotype (G–J). (E,F) Quantification of the multiple wing hair phenotypes in response to RNAi leading to knockdown of *cip4* or *nostrin* (E) and in mutants (F). The percentage of cells with two or more than three wing hairs was counted posterior of the fifth longitudinal vein. $n>6000$ cells per genotype. *P*-values were calculated using the Student's *t*-test; ***≤0.001; *≤0.1. (K,L) Still images taken from a time-lapse movie of a pupal wing expressing Nostrin–EGFP at 26 h (K) and at 32 h APF (L). Distal is right and proximal is left. (M–O) 3D-reconstruction of a structured illumination microscopy (SIM) image of a pupal wing expressing Nostrin–EGFP (green) stained for microtubules (red). (P,Q) The asymmetric localization of Frizzled is not affected in *nost;;cip4* double mutant wings (28 h APF). (R–R″). *nost;;cip4* double mutant pupal wing 32 h APF stained for Frizzled (green) and F-actin (red). Scale bars: 25 (m (A–D and G–J), 5 μm (K,L,P–R), 1 μm (M–O).

Journal of Cell Science (2015) 128, 499–515 doi:10.1242/jcs.155929

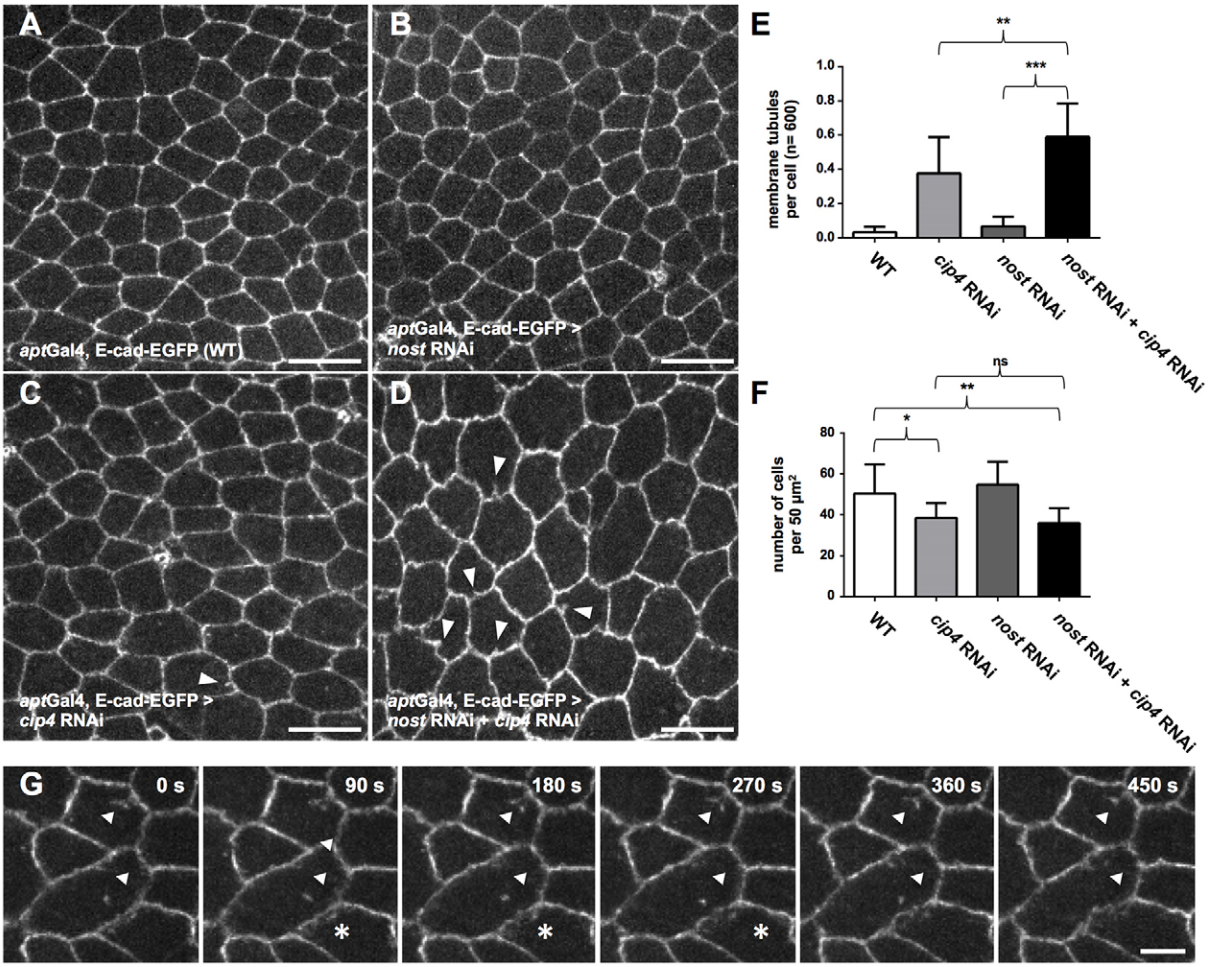

Fig. 3. Loss of *nostrin* and *cip4* gene functions affect E-cadherin trafficking *in vivo*. (A–D) Single frames of spinning disk microscopy time-lapse movies of *in vivo* E-cadherin–EGFP expression driven by the *apterous*Gal4 driver in dorsal thorax epithelium of 17 APF pupae (See also supplementary material Movies 3–6). Genotypes as indicated, scale bar: 10 µm. (E) Quantification of membrane tubules per cell. Time-lapse movies were blind-scored. Knockdown of *cip4* leads to an increase in the number of tubules per cell. Additional knockdown of *nostrin* strongly enhances this phenotype. Furthermore *cip4* knockdown and *nost;;cip4* double knockdown leads to an increase in cell size (F). Error bars represent standard deviation, *P*-values were calculated using one-way ANOVA (*$P<0.05$, **$P<0.01$, ***$P<0.001$). (G) Single frames of spinning disk microscopy of E-cadherin–EGFP *in vivo* in *nostrin* RNAi, *cip4* RNAi background. Time points as indicated. Arrowheads indicate tubule formation. The asterisk marks the detachment of neighboring membranes (see also supplementary material Movie 6b). Scale bar: 5 µm.

Since defects in the differentiation of follicle cells can lead to fused egg chambers (Horne-Badovinac and Bilder, 2005), we further analyzed double mutant egg chambers in more detail. The encapsulation defect of *nost;;cip4* double mutants is not caused by follicle cell differentiation defects that result in fused egg chambers as previously found for instance in mutants defective for Notch/Delta signaling (López-Schier and St Johnston, 2001). Multicyst (so called 'compound') *nost;;cip4* mutant egg chambers are enveloped by a regular follicular epithelium and separated by interfollicular stalk cells. The polar cells of mutant egg chambers are located at opposing sides as in wild type, but can also be found at lateral positions (Fig. 4I–K).

Loss of *cip4* and *nostrin* disrupts the morphology of the germarium

The encapsulation defect of germline cysts is already obvious from the defective morphology of *nost;;cip4* mutant germaria (Fig. 5E). The wild type germarium can be subdivided in four regions, denoted from the anterior to posterior site as regions 1, 2a, 2b and 3 (Fig. 5A). In region 2a the cyst already contains 16 germ cells and forms a cluster of round cells. When the cyst enters region 2b, it forms a lens-like structure and gets surrounded by follicle cells. As the cyst moves along the germarium from region 2b to region 3, it finally buds off as a single egg chamber (Fig. 5A). No striking differences were found in single *nostrin* or *cip4* mutant germaria (Fig. 5C,D). In contrast, double mutant germaria do not form such lens-like structures (Fig. 5E, asterisk) and cysts are stringed in region 2b (Fig. 5E, arrows). Previous studies revealed that the underlying cell rearrangement during cyst flattening depends on homophillic E-cadherin–dependent adhesion between the germline cells (Godt and Tepass, 1998; González-Reyes and St Johnston, 1998). The flattening of the cyst is in turn a prerequisite for the correct positioning of the oocyte (Godt and Tepass, 1998). Accordingly, germline clones for the E-cadherin encoding gene *shotgun* (*shg*) show defects in cyst flattening in region 2B and a mispositioning of the oocyte in the germarium similar to defects observed in *nost;;cip4* double mutants (McCaffrey et al., 2006).

Journal of Cell Science (2015) 128, 499–515 doi:10.1242/jcs.155929

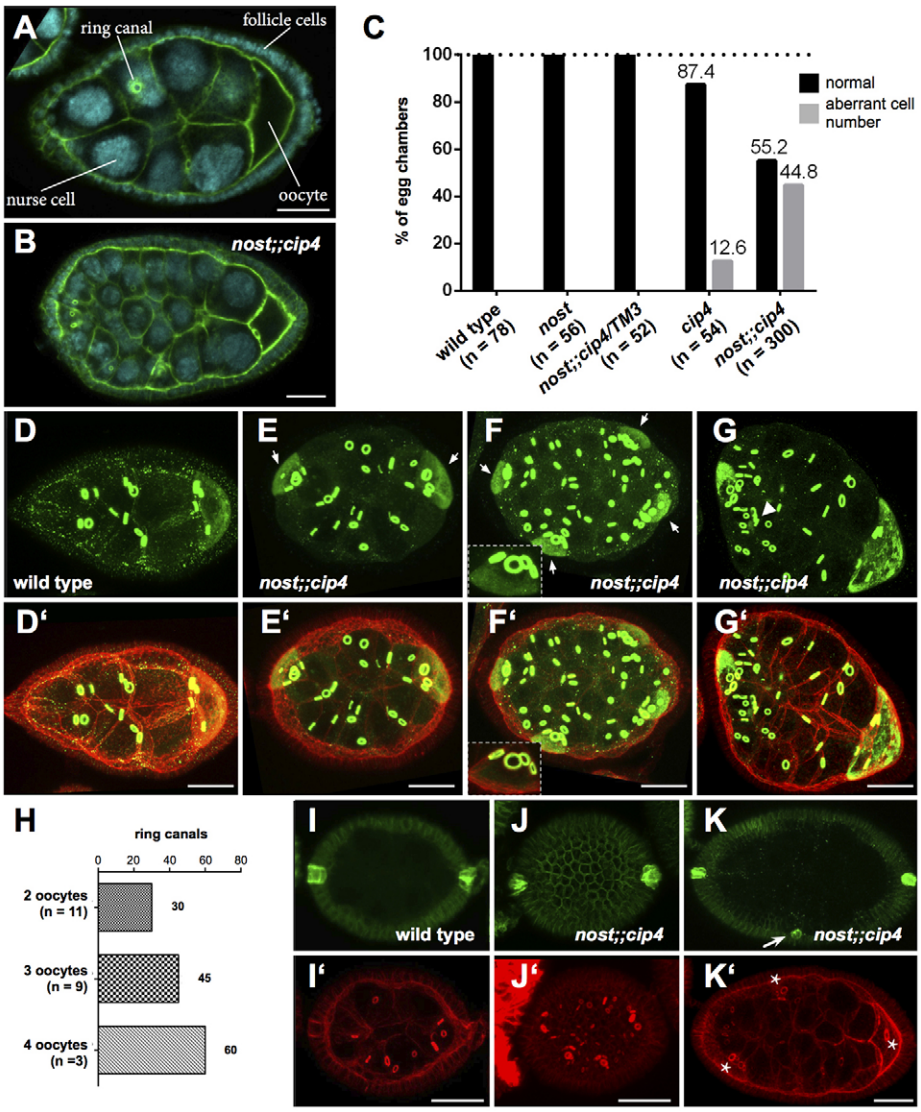

Fig. 4. *nost;;cip4* double mutant egg chambers show an aberrant number of germline cells. (A) Wild type egg chamber stage 7 with 15 germline cells and one oocyte surrounded by a follicle cell epithelium. (B) *nost;;cip4* mutant egg chambers contain an aberrant number of germline cells (F-actin, green and DAPI, blue). (C) Quantification of defective egg chambers of the indicated genotypes. (D–G′) Maximum intensity projections of egg chambers stained with htsRC (ring canals, green), orb (oocytes, green) and phalloidin (F-actin, red). A stage 7 wild type egg chamber contains one oocyte at the posterior and 15 ring canals connecting the germ cells, whereas double mutants show multiple oocytes and an aberrant number of ring canals. The magnifications in F,F′ in the dotted boxes show that the oocytes always contain four ring canals. Arrows in E and F mark the position of oocytes. Arrowhead in G marks an ectopic oocyte in a more central position. (H) Ring canals were counted in *nost;;cip4* mutant egg chambers. The number of ring canals correlates with the expected number for an encapsulation defect. (I–K) Maximum intensity projection of wild type and mutant egg chambers stained for phalloidin (F-actin, red) and for FasIII to visualize polar cells (green). Arrow in K marks the position of ectopic polar cells. Asterisks in K′ mark the position of oocytes. Scale bars: 20 μm.

Remarkably, we found the strongest expression of endogenous Nostrin protein in wild type germline cyst cells in region 2a (Fig. 5F–G″). Co-immunostaining with Fasciclin III, a cell adhesion molecule that is found the most in immature follicle cells in the germarium, clearly shows that Nostrin specifically accumulates in germ cells at the border between region 2a and 2b, before somatic follicle cells start to encapsulate individual germline cysts (Fig. 5I; supplementary material Movie 7). In some wild type germaria weaker expression could also be observed in germ cells in region 3 (Fig. 5H). No significant staining was found in germarial region 2b or in late egg chamber stages, neither in the germline nor in the somatic follicle epithelium (compared to *nos* mutant egg chambers in Fig. 5F). Compared to Nostrin, Cip4 is more broadly expressed (supplementary material Fig. S2). Highest expression of endogenous Cip4 is found in germ cells of all germarial regions (2a, 2b and 3) but also although weaker in somatic follicle cells (supplementary material Fig. S2).

Loss of both *cip4* and *nostrin* affects the localization of E-cadherin in egg chambers

Based on the finding that Cip4 and Nostrin cooperatively regulate E-cadherin membrane turnover in the thorax epithelium, we determined the localization of E-cadherin in double mutant germaria and early compound egg chambers. E-cadherin is normally located in the membranes of germline cells and in the apical-lateral membrane of the follicle cells from germarial region 2 onwards (Fig. 6; Godt and Tepass, 1998; González-Reyes and St Johnston, 1992). In wild type germaria, high levels of E-cadherin are found in the area of contact between the oocyte and the follicle cells at the posterior pole as previously reported (Godt and Tepass, 1998; González-Reyes and St Johnston, 1998). In later stages, E-cadherin is enriched in the lateral follicle membrane and highly concentrated in patches between the apical side of follicle cells and the germ cells. In contrast, *nost;;cip4* double mutant germaria show an overall reduced E-cadherin staining (Fig. 6C). Significant differences of E-cadherin localization are most apparent in stage 1–6 mutant egg chambers, where the enrichment of E-cadherin between germ and follicle cells is clearly reduced (Fig. 6B,D, quantified in Fig. 6E). The localization at lateral follicle membranes is not affected. The reduced apical E-cadherin localization in follicle cells might be due to a loss of homophillic binding partners in the germline. Remarkably, we found that the apical localization of Armadillo/β-catenin, which

Journal of Cell Science (2015) 128, 499–515 doi:10.1242/jcs.155929

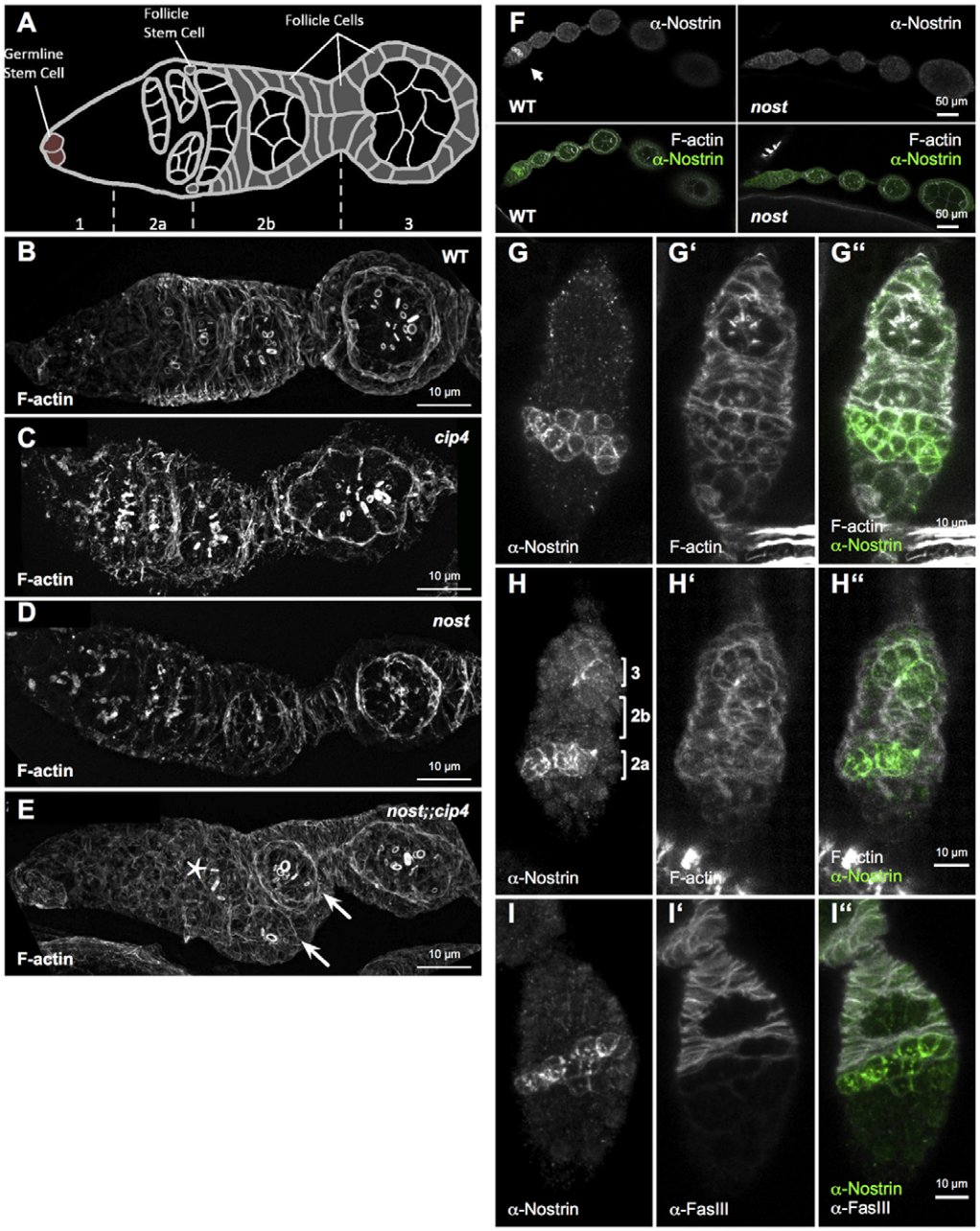

Fig. 5. *nost;;cip4* double mutant germaria show morphological defects. (A) Drawing of a wild type germarium. The different regions of the germarium are indicated. Germline cysts form a typical lens-like structure between regions 2a and 2b, before they get surrounded by follicle cells in region 2b and bud off as an egg chamber in region 3. The egg chambers mature progressively towards the posterior. Each of them consists of 16 cells, one oocyte and 15 nurse cells, enveloped by a monolayered follicle cell epithelium. (B–E) Maximum-intensity projections of SIM images of germaria stained with phalloidin to visualize the overall morphology. Genotypes are indicated. *nost* or *cip4* single mutants show no obvious morphological defects, whereas double mutant germaria show several morphological defects like two cysts side by side in region 2b (E, arrows) and the absence of the lens-like structure in region 2b (E, asterisk). (F) Confocal images of wild type (left panel) and (right panel) *nostrin* ovarioles stained for Nostrin and F-actin. Nostrin specifically localizes to a distinct cell population in the germarium (marked by the arrow). (G–G″) Confocal images (maximum intensity projection of six planes) of a wild type germarium stained for Nostrin (green) and F-actin. Nostrin specifically accumulates in germ cells in germarial region 2a. (H–H″) In some wild type germaria weaker expression could also be observed in germ cells in region 3. No significant signals were found in germarial region 2b or in later egg chamber stages. (I–I″) Confocal images (maximum intensity projection of six single sections) of a wild type germarium stained for Nostrin and FasIII. Nostrin is strongly expressed at the cell borders between region 2a and 2b, whereas FasIII marks follicle cells in regions 2b and 3. Scale bars: (A–E) 10 µm (A-E, G–I), 50 µm (F).

forms a cell adhesion complex with E-cadherin, seems unaffected in *nost;;cip4* double mutant egg chambers (Fig. 6B,D). This suggests that E-cadherin is not absolutely essential for the formation of a cadherin–catenin complex at adherent junctions between germ and follicle cells. Previous studies suggested that alternative adhesion systems such as N-cadherin might compensate for the loss of E-cadherin (Tanentzapf et al., 2000).

Thus, our data suggest that an impaired membrane turnover of E-cadherin in *nost;;cip4* germ cells might affect the homophilic

Journal of Cell Science (2015) 128, 499–515 doi:10.1242/jcs.155929

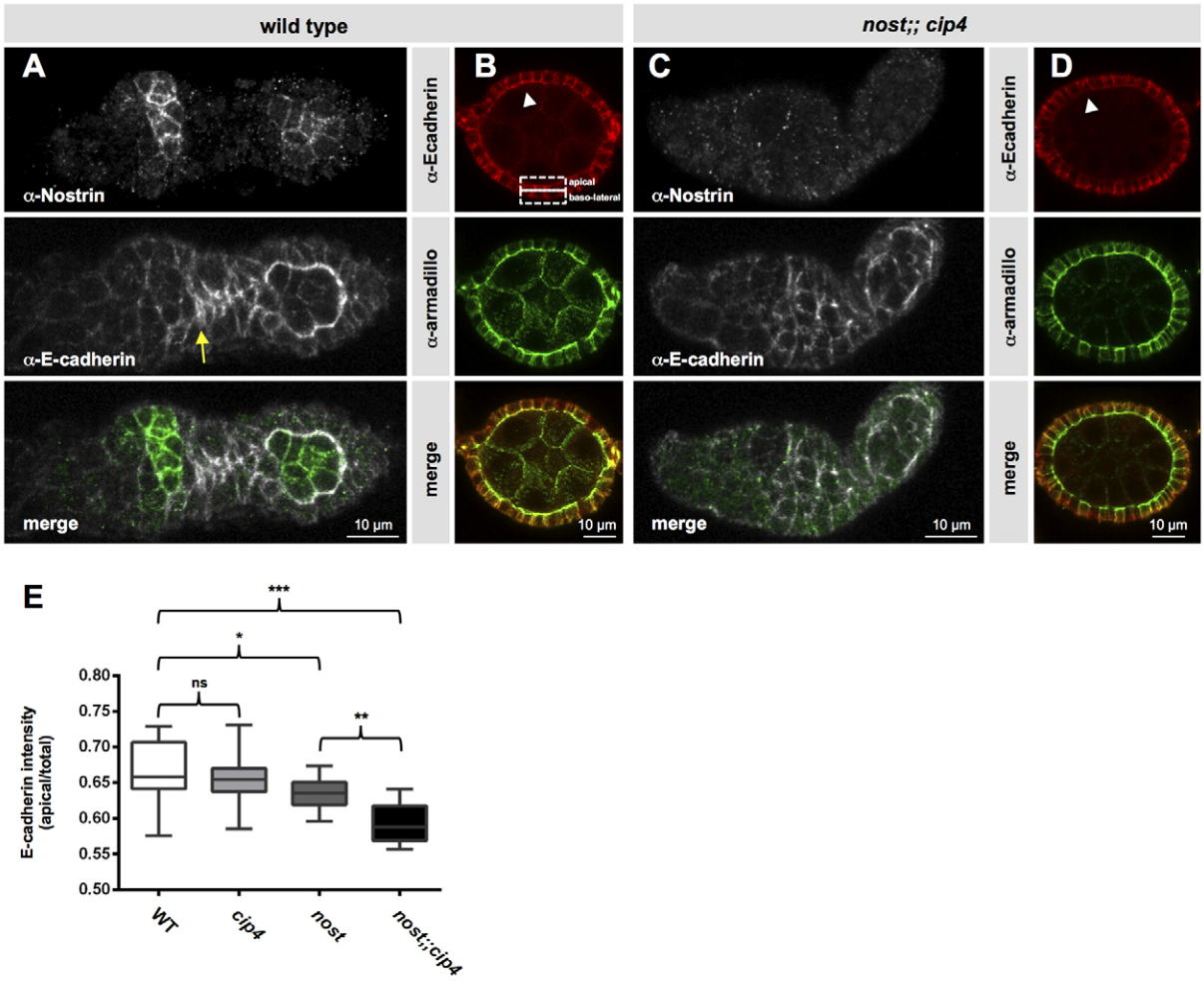

Fig. 6. Loss of both *nostrin* and *cip4* affect the apical localization of E-cadherin. Maximum-intensity projection (five confocal sections of germaria and stage 4 egg chambers). (A) Wild type germarium stained for Nostrin and E-cadherin. The yellow arrow marks the E-cadherin enrichment at the posterior region of contact between the oocyte and the follicle cells. (B) Wild type stage 4 egg chamber stained for Armadillo and E-cadherin; arrowhead indicates xxxxxxxxxxxx. (C) *nost;;cip4* mutant germarium stained for Nostrin and E-cadherin. (D) *nost;;cip4* mutant stage 4 egg chamber stained for Armadillo and E-cadherin. In wild type, E-cadherin localizes at the lateral and apical membrane in close contact to the germline cells. Between the germline cells only a weak signal for E-cadherin is detectable. In germline cysts of double mutants as well as in stage 4 egg chambers (arrowhead), the E-cadherin signal between follicle and germline cells is strongly reduced, whereas the lateral localization of E-cadherin in follicle cells seems not to be affected. Armadillo/β-catenin localization at the apical membrane of follicle cells seems not to be affected. (E) Quantification of the E-cadherin localization. The average intensities of E-cadherin were measured at the border between germline and follicle cells, and normalized against the total E-cadherin intensity; the selected area of measurement is indicated in B (3 µm×11 µm rectangle). Whiskers indicate minimum and maximum values. *P*-values were calculated using one-way ANOVA (*$P<0.05$, **$P<0.01$, ***$P<0.001$). Scale bars: 10 µm (A–D).

adhesion between follicle and germline cells resulting in encapsulation defects and oocyte mispositioning.

Cip4 and Nostrin do not form heterodimers but localize at the same tubular structures in cells

The phenotypic analysis of double mutants revealed a cooperative function of Cip4 and Nostrin *in vivo*. We thus next addressed whether Cip4 and Nostrin may just functionally cooperate or directly act together as F-BAR heterooligomers. GST-pull-down assays only revealed a weak interaction between Nostrin and Cip4 when compared to the interaction of Cip4 with WASP (Fig. 7A). We thus concluded that this interaction may rather be indirect than mediated by F-BAR heterodimers. Consistently, we could only detect Nostrin dimerization but not a direct interaction between Cip4 and Nostrin using the *Bimolecular Fluorescence Complementation* (BiFC) technique (Gohl et al., 2010); supplementary material Fig. S3). Control experiments with Cip4 and WASP, that yielded a positive signal (supplementary material Fig. S3), confirmed that the Cip4 constructs used were active.

In line with this observation, we found a differential localization of Cip4 and Nostrin in *Drosophila* S2R+ cells. Cip4 mainly localizes at the cell's leading edge and at dynamic Rab5 positive endocytic vesicles driven by actin comet tails (Fricke et al., 2009). Nostrin does not overlap with F-actin. Instead, EGFP-fused Nostrin protein marks small vesicles that preferentially seem to move along microtubules (Fig. 7B,C; supplementary material Movies 8, 9). Co-transfection experiments show a strong co-localization of Nostrin with Rab11-positive endosomes (Fig. 7D; supplementary material Movie 10). However, a more careful analysis suggests that Cip4 and Nostrin may show some spatial overlap, as Nostrin also partially co-localizes with Rab5 (Fig. 7E; supplementary material Movie 11).

Journal of Cell Science (2015) 128, 499–515 doi:10.1242/jcs.155929

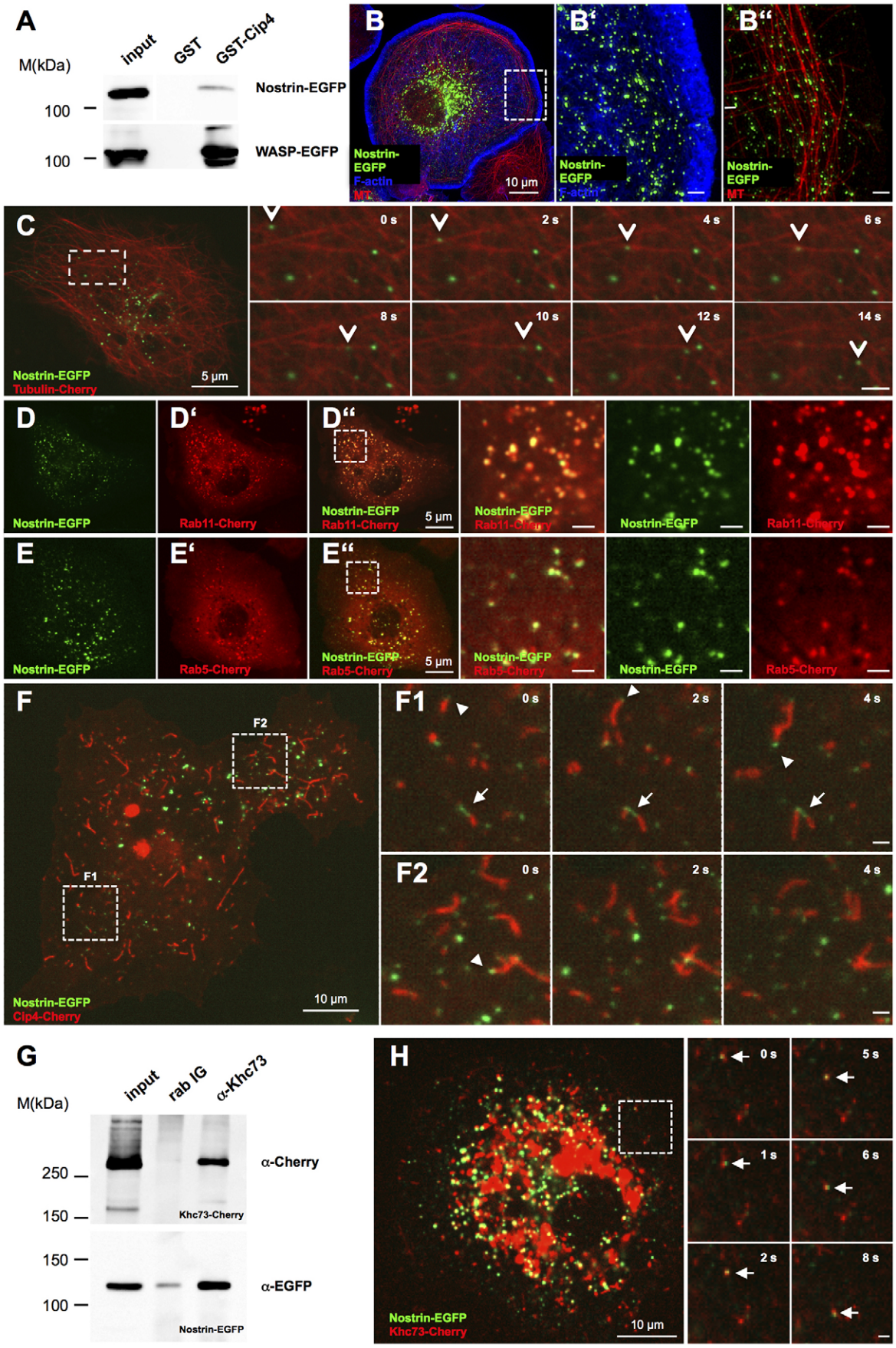

Fig. 7. See next page for legend.

Journal of Cell Science (2015) 128, 499–515 doi:10.1242/jcs.155929

Fig. 7. Nostrin and Cip4 localize to distinct domains of the endosomal compartment. (A) GST pull-down with GST–Cip4 or GST coupled to glutathione beads incubated with extracts of S2R+ cells expressing either Nostrin–EGFP or WASP–EGFP. (B–B″) SIM image of an S2R+ cell transfected with Nostrin–EGFP (green) stained for F-actin (blue) and microtubules (Tubstain; Theiss et al., 2012, in red). A magnification of the framed region in B is shown in B′ and B″. Nostrin–EGFP-positive vesicles frequently localize at microtubules. (C) Single frames of a spinning disk microscopy time-lapse movie of an S2R+ cell transfected with Nostrin–EGFP (green) and Tubulin-Cherry (red). See also supplementary material Movie 9. (D,E) Still images of time-lapse movies of S2R+ cells transfected with Nostrin–EGFP (green) and (D) Rab11-Cherry (red) or (E) Rab5-Cherry (red), respectively. See also supplementary material Movies 10 and 11. (F) Single frames of a spinning disk microscopy time-lapse movie of an S2R+ cell transfected with Nostrin–EGFP (green) and Cip4-Cherry (red). (F1,F2) Magnifications of indicated regions. Arrowheads mark the localization of Nostrin at the tips of Cip4-induced tubules; arrows mark the position of Nostrin in between Cip4 marked structures. See also supplementary material Movie 12. (G) Co-immunoprecipitation of Nostrin with Khc73. EGFP-tagged Nostrin and Cherry-tagged Khc73 constructs were co-transfected into S2R+ cells and cell lysates were immunoprecipitated with a control preimmune serum or an anti-Khc antibody. The immunoprecipitates were probed for the presence of Khc73-Cherry (anti-Cherry antibody) and Nostrin–EGFP (anti-EGFP antibody) as indicated. Scale bars: 10 μm (B,C,F,H); 5 μm (D–E″); 1 μm [B′,B″; and movie frames of the indicated regions in C, F (F1,F2) and H].

In order to directly visualize whether Cip4 and Nostrin might act together at endosomal membrane compartments we co-expressed Cip4–EGFP and Nostrin–Cherry and analyzed the dynamic tubular membrane structures induced by Cip4 expression (Fricke et al., 2009) using spinning disk microscopy. Remarkably, Nostrin is found at the tips of Cip4 induced membrane tubules or localizes in between Cip4 marked structures (Fig. 7F1,F2; supplementary material Movie 12). Co-immunostaining of co-transfected cells for endogenous Rab11 suggest that only subpopulations of Rab11-positive endosomes co-localize with Cip4–EGFP and Nostrin–Cherry (supplementary material Fig. S4A). Interestingly, recent studies identified a mechanism of Rab11-dependent recycling endosome tubule morphogenesis that requires the kinesin motor protein Kif13A (Delevoye et al., 2014). Thus, we further analyzed a possible co-localization between Nostrin and the *Drosophila* Kif13A homologue Khc73, a known processive microtubule plus end-directed motor that colocalizes with endosomal vesicles (Huckaba et al., 2011). And indeed, we found that Nostrin physically interacts with Khc73 but it also strongly co-localizes with Khc73-marked endosomes moving along microtubules (Fig. 7G,H and supplementary material Movie 13). Additionally, Nostrin and Khc73 are often enriched at the peripheral tips of microtubules at the cell periphery as recently described for a Khc73–EGFP construct (Huckaba et al., 2011; supplementary material Movie 14).

Cip4 and Nostrin directly bind membranes with different lipid binding preferences

Since Cip4 and Nostrin seem to display preferences for distinct subdomains of communicating membrane compartments *in vivo*, we analyzed the membrane association of Cip4 and Nostrin in a direct manner by subjecting recombinant proteins to liposome floatation assays. In controls without liposomes, both Cip4 and Nostrin remained at the bottom of the density gradients (Fig. 8A; fractions 4–6). In contrast, with liposomes generated from Folch-fraction I added, Cip4 and Nostrin floated together with the liposomes (Fig. 8A; liposomes floated to fraction 2 or 3 depending on liposome preparation, as determined by direct liposome visualization). GST used as a control did not associate with the floating liposomes. Thus, both F-BAR proteins directly bind to membranes. Cip4 and Nostrin associated with cholesterol-based (70% cholesterol), phosphatidylcholine (PC)-containing (20% PC) liposomes supplemented with the lipid phosphatidylserine (PS; 10% PS).

Similar to other F-BAR domain proteins, such as Syndapin I and II (Dharmalingam et al., 2009), Nostrin failed to associate with liposomes only composed of phosphatidylethanolamine (PE; 80% PE) and phosphatidylcholine (PC; 20% PC). Surprisingly, Cip4 behaves differently compared with all F-BAR domain proteins analyzed so far. Cip4 robustly interacts with PE/PC liposomes, as seen in liposome floatation analyses [Fig. 8A; liposome-containing fraction, F3 (asterisk)]. Thus, Cip4 and Nostrin show different lipid-binding preferences.

Cip4 and Nostrin prefer similar membrane curvatures but form different types of lattice

BAR domains are membrane-topology-sensing and/or -inducing modules (Qualmann et al., 2011). Given that Cip4 overexpression tubulates membranes in S2R+ cells but Nostrin overexpression does not (Fricke et al., 2009), we next used electron microscopy to analyze liposomes coated by either Cip4 or Nostrin. In samples subjected to freeze-fracture analyses and also in cryo-EM experiments, we observed that both proteins convert liposomes into smaller structures of completely different shape (Fig. 8C,D), whereas in control reactions, liposomes had usually a diameter of several hundreds of nanometers (Fig. 8B; GST control). Thus, both Cip4 and Nostrin induce vesiculo-tubular membrane structures.

Quantification of the cryo-EM-determined tubule diameters in the presence of Cip4 or Nostrin (Fig. 8E–G) showed that both proteins induce tubules to a similar extend; Nostrin, 0.45 tubules/vesicles (190:421); Cip4 0.41 tubules/vesicles (196:484). Association with both F-BAR proteins leads to relatively well-defined membrane curvatures. Cip4-induced tubules have a diameter ranging from 48–86 nm. Nostrin showed slightly less-restricted preferences, as the diameters varied between 39 and 109 nm. Yet, on average, both proteins prefer membrane curvatures with an diameter of ~70 nm, i.e. both induce almost identical curvatures (quantified in Fig. 8H).

We next tested a combination of Nostrin and Cip4 for *in vitro* tubulation. To exclude any tag-mediated heterooligomerization, we first liberated Cip4 from its GST-tag by incubation with precision protease. Untagged Cip4 protein still binds to liposomes (supplementary material Fig. S4C) and induces mean tubule diameters of ~74 nm. The tubular structures formed by Cip4 and Nostrin together are indistinguishable from those formed by the individual proteins (Fig. 8G,H).

Since both proteins effectively bind to membranes, induce similar curvatures, but display slightly different curvature ranges *in vitro*, we next asked whether any differences in Cip4 and Nostrin lattice formation could be detected at the membrane surfaces. Liposomal membranes incubated with Nostrin appear smooth. Neither in freeze-fracture analyses nor in high-resolution cryo-EM any obvious protein coat was detected (Fig. 8I). In contrast, liposomes incubated with Cip4 in many cases display material at the edges of freeze-fractures. This material appears as discrete, relatively globularly shaped structures of roughly 10–20 nm in diameter that, if detectable, often appears as continuous strings along tubular structures (Fig. 8J). Higher-resolution imaging reveals that the electron-dense material often has a regular tip-to-tip spacing of about 20 nm (Fig. 8J, right panels).

Journal of Cell Science (2015) 128, 499–515 doi:10.1242/jcs.155929

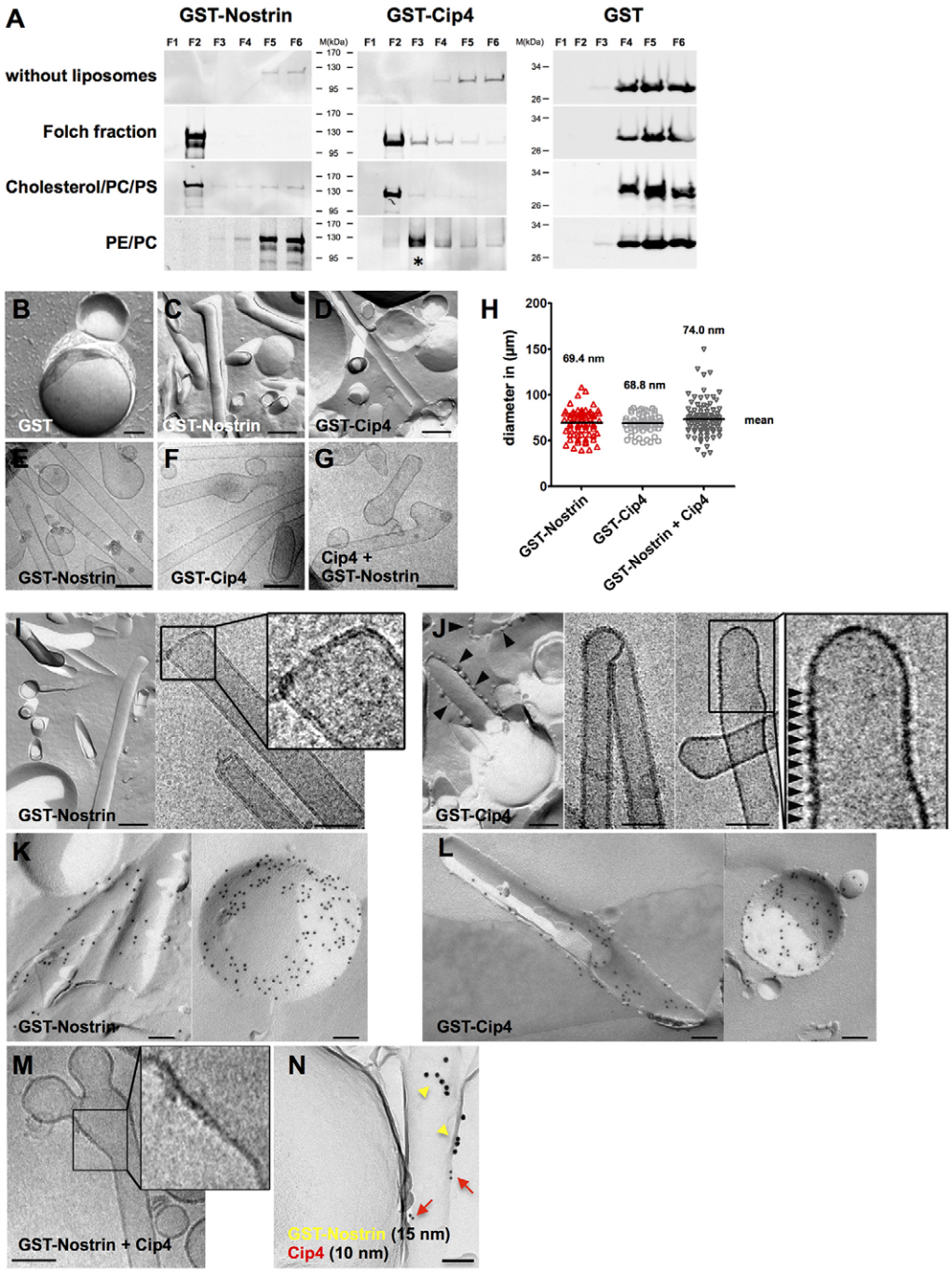

Fig. 8. See next page for legend.

We hypothesized that the regular arrays at liposomes incubated with Cip4 represent regular protein lattices formed upon F-BAR domain self-association. Since such patterns are not observable at tubular structures in Nostrin incubations, we wondered whether both proteins form membrane tubules by different mechanisms or whether in both cases tubules would be protein-decorated but Nostrin molecules simply adopt more random organizations at the membranes. In order to address this, we subjected the liposomes incubated with Cip4 and Nostrin, respectively, to anti-GST immunogold labeling of freeze-fracture replica. Both proteins were successfully and specifically detected. No labeling was obtained in GST controls (data not shown). Interestingly, both Cip4 and Nostrin appear to be uniformly distributed along tubular and vesicular structures (Fig. 8K,L).

Finally, we analyzed liposomes incubated with both GST–Nostrin and Cip4 (GST–Nostrin + Cip4) in more detail and studied the distribution of both proteins in freeze-fractured samples using a double immunogold approach. Higher resolution analyses of GST–Nostrin + Cip4 liposomes, again, showed areas decorated with the regular structures protruding from the surface of membrane tubules, as seen for GST–Cip4 alone (Fig. 8M). Adjacent membrane areas often appeared smoother. Strikingly, the anti-GST (for GST-Nostrin) and the Cip4 immunogoldsignals are not intermingled but are either found on different vesicular

Journal of Cell Science (2015) 128, 499–515 doi:10.1242/jcs.155929

Fig. 8. Cip4 and Nostrin give rise to tubular membrane structures of similar mean diameters. (A) Liposome floatation analyses of recombinant GST, GST–Nostrin and GST–Cip4 proteins with liposomes composed of different membrane lipids as indicated. Six density-gradient fractions (F1 to F6) were immunoblotted with anti-GST antibodies. Liposomes normally floated into fraction 2, except for PE/PC liposomes (F3 marked by an asterisk) as proven by incorporation of fluorescently labeled lipids (not shown). Note that GST–Cip4 but not GST–Nostrin strongly associates with PE/PC-containing liposomes. (B) Electron micrographs of freeze-fractured incubations of liposomes generated from Folch fraction type I lipids, incubated with GST, as control, (C) GST–Nostrin, (D) GST–Cip4. Scale bars: 200 nm. (E–G) Cryo-TEM images of liposome–protein incubations. Scale bars: 200 nm. Note that a combination of GST–Nostrin and Cip4 induces tubular structures that are similar to those induced by GST-Nostrin or GST-Cip4 alone. (H) Quantification of the diameters of tubular membrane structures induced by recombinant GST-Nostrin, GST-Cip4 and a combination of GST-Nostrin and Cip4, respectively, as observed by Cryo-TEM. $n=66$–71 tubular structures. (I,J) Replica of freeze-fractured liposomes visualized by TEM and CryoEM of liposomes incubated with (I) GST–Nostrin, (J) GST–Cip4; scale bars: 100 nm. Insets represent magnifications of boxed areas. Note that tubular structures formed in incubations with Nostrin appear to have smooth surfaces, whereas those incubated with CIP4 often show material at their membrane surface (arrowheads). Analyses at higher magnifications (see insets) show a regular pattern of electron-dense aggregates at the surface of liposome tubules with a spacing of about 20 nm (measured tip-to-tip; arrowheads). (K,L) High-resolution analysis of anti-GST immunogold-labeled, freeze-fractured liposomes incubated with (K) GST–Nostrin and (L) GST–Cip4. Both Nostrin and CIP4 were found to relatively uniformly decorate the surface of both tubular and vesicular structures. Scale bars: 100 nm. (M) Replica of freeze-fractured liposomes incubated with Cip4 and GST–Nostrin (scale bar: 100 nm). Insets represent magnifications of boxed areas. (N) Double-labeling of freeze-fractured liposomes incubated with GST-Nostrin and Cip4 using antibodies conjugated to 10-nm (Cip4, marked by red arrows) or 15-nm (Nostrin, marked by yellow arrowheads) colloidal gold. Strikingly, the immunogold signals seem not to be intermingled, but segregate into different areas within vesiculo-tubular structures. Scale bar: 100 nm.

and tubular structures or, in case they are both found on lipid structures, they are present in segregated zones of tubular structures (Fig. 8N).

In summary, the different abilities of Cip4 and Nostrin in tubulation *in vivo*, the different diameter ranges of Cip4- and Nostrin-decorated vesiculo-tubular structures, the different appearance of the protein coats, and finally the observation that both proteins occur in a segregated manner suggest that Nostrin and Cip4 organize distinct membrane areas. However, both F-BAR proteins prefer similar curvatures and can be directly adjacent to each other, an observation that might explain the strong cooperative function in the regulation of E-cadherin membrane trafficking observed *in vivo*.

DISCUSSION

Structural, biochemical and cell culture analyses have led to a comprehensive molecular understanding of how F-BAR proteins might be involved in membrane deformation and endocytosis. These data support an important role for F-BAR proteins in the regulation of membrane curvatures in a sequential manner during endocytosis (Suetsugu, 2010). Despite their pivotal functions in linking actin and membrane dynamics, recent single-knockout studies revealed that many F-BAR proteins are not essential for development and, thus, might have redundant or cooperative functions *in vivo* (Feng et al., 2010; Fricke et al., 2009). In fission yeast, the Cip4-like F-BAR proteins Cdc15 and Imp2 are examples for such synergistic function of two F-BAR proteins. Cells deficient for either Cdc15 or Imp2 show mild defects in cytokinesis but are still able to divide (Demeter and Sazer, 1998; Fankhauser et al., 1995). However, deletion of both C-terminal SH3 domains of the proteins completely restricts the division of the cells (Roberts-Galbraith et al., 2009).

Nostrin and Cip4 regulate membrane localization of E-cadherin to coordinate packing of the egg chamber

In our work here, we provide first evidence for cooperative function of the two F-BAR proteins Cip4 and Nostrin in the multicellular context of *Drosophila* development. Like Cip4, members of the Nostrin subfamily show a remarkably high evolutionary conservation and single orthologs can be found from porifera to humans. All the more surprising is the fact that *nostrin* loss-of-function mutant flies have no obvious phenotype. Only after removal of both *cip4* and *nostrin*, we found a strong enhancement of the phenotypic traits already observed in *cip4* single mutants. Double mutants show a substantial reduction in the number of offspring. Both mutant females and males display reduced fertility, indicating a common function of both F-BAR proteins in early morphogenesis. Female sterility of double mutant flies is caused by strong defects in egg chamber morphogenesis. The formation of compound egg chambers results from a defective encapsulation in the germarium, a phenotype that has not yet been described for many mutants. Most mutations that have been reported of so far, either affect gene functions directly through the regulation of cell division or control of follicle cell differentiation through Notch/Delta signaling (Grammont and Irvine, 2001; López-Schier and St Johnston, 2001; Vachias et al., 2010). However, multicyst egg chambers in *nost;;cip4* double mutants display neither defects in cell division nor in the differentiation of follicle cells.

Interestingly, loss of Maelstrom (Mael), a high-mobility group box protein that regulates microtubule organization leads to egg chambers with cell division defects but also results in an encapsulation defect with misplaced oocytes that is similar to the one observed in *nost;;cip4* double mutants (Sato et al., 2011). Mael forms a complex with the components of the microtubule-organizing center (MTOC) – including centrosomin and γ-tubulin, which seems to be required not only for early oocyte determination but also egg chamber packing and oocyte positioning in the germarium. Interestingly, in *mael* mutant multicyst egg chambers E-cadherin is not enriched on the oocyte cortex and not apically concentrated in the follicle epithelium as in wild type. *nost;;cip4* double mutant egg chambers show a similar E-cadherin mislocalization, suggesting that the microtuble cytoskeleton plays an important role in E-cadherin localization. Consistently, we found that Nostrin mainly localizes to Rab11-positive vesicles that move along microtubules. Thus, Nostrin might act on Rab11-dependent E-cadherin trafficking along microtubules. A strong requirement for Rab11 in E-cadherin trafficking in germline stem cells (GSC) and in the maintenance of GSC identity has recently been identified (Xu et al., 2011). Mosaic egg chambers are severely disorganized, comprising mispositioned oocytes. Most importantly, compound egg chambers can be found that contain two or more germline cysts surrounded by a single continuous follicle epithelium, as we observe here for *nost;;cip4* mutants (Bogard et al., 2007; Xu et al., 2011). However, *rab11*-null follicle stem cells (FSC) give rise to the normal number of cells that enter polar, stalk and epithelial cell differentiation pathways (Xu et al., 2011). Like Rab11, Nostrin and Cip4 functions do not seem to be required in follicle cell differentiation.

Journal of Cell Science (2015) 128, 499–515 doi:10.1242/jcs.155929

Given the dramatic switch in Nostrin expression in the germline cysts between region 2a and region 2b, when protein levels drop from highest to very low or no expression (Fig. 5H), we propose an important function of Nostrin in germ cells rather than in somatic follicle cells. The germline cyst undergoes a dramatic change in shape within this region, as is reflected by a transformation from a spherical to a lens-shaped structure. This morphological transition might imply important changes in the adhesiveness mediated by homophilic E-cadherin cell-cell contacts between germ cells within the cyst. Thus, we propose that Nostrin and Cip4 are involved in the regulation of this transition by controlling E-cadherin endocytosis and vesicle recycling in germline cells. A failure of *nost;;cip4* mutant cysts in adopting a lens-shaped morphology might interfere with their encapsulation by follicle cells, which results in the formation of compound egg chambers.

Given the substantial mislocalization of E-cadherin that becomes obvious in double mutant egg chambers, we further suggest an additional role of both F-BAR proteins in the maintenance of E-cadherin cell–cell contacts between germline and somatic follicle cells.

Nostrin might function at endosomal tubule intermediates mediating microtubule-dependent trafficking of recycling endosomes

Cip4 and Nostrin partially mark the same membrane structures but they localize to distinct subregions *in vivo*. Consistently, our *in vitro* liposome studies showed that both proteins prefer defined membrane curvatures of similar diameter, i.e. both might associate with similarly shaped membrane compartments. However, the different appearance of Cip4- and Nostrin-decorated vesiculo-tubular structures might also reflect differences in lattice formation of these two F-BAR domain proteins. We hypothesize that these regular arrays of electron-dense structures at liposomes represent regular Cip4 lattices formed upon self-association by head-to-tail and lateral interactions as previously supposed by real-space reconstruction (Frost et al., 2008). Because such patterns were not observed at tubular structures following incubation in the presence of Nostrin, we suggest that Nostrin does not polymerize into rigid helical coats that are thought to be the structural basis for membrane invagination. Consistently, unlike Cip4, overexpression of Nostrin in S2R+ cells did not induce membrane tubulation (Fricke et al., 2009). How do Cip4 and Nostrin cooperate in membrane remodeling and vesicle trafficking? In cells, Cip4 mainly localizes to Rab5-positive early endosomes (Fricke et al., 2009), whereas Nostrin marks both Rab5- and Rab11-positive vesicles. Thus, we propose a cooperative recruitment model, in which first Cip4 promotes membrane invagination, vesicle scission and motility of Rab5-positive membrane compartments by recruiting dynamin and the WASP–WAVE–Arp2/3 pathway. Nostrin will then be recruited to Cip4-positive membrane structures because Nostrin prefers the curvature induced by the highly organized Cip4 coats. Yet, at these membrane compartments, both proteins still occur in a spatially segregated manner, as visualized in our EM analyses of Cip4- and Nostrin-coated membrane tubules. This segregation might reflect that Nostrin is not interacting with Cip4, and that Cip4 has the ability to bind PE – which Nostrin does not have. Furthermore Nostrin protein arrays seem less organized, as reflected by the broader range of curvatures induced *in vitro* and by the lack of regular structures of Nostrin-coated membranes. Strong formation of rigid lattices might explain why Cip4 tubulates membranes effectively *in vitro* and *in vivo*, and why anti-Cip4 labeling usually outlines tubular structures. In contrast, Nostrin is confined to Cip4-free segments of these structures and predominantly appears at the end of such Cip4-coated tubules because the end does not accommodate a Cip4 coat optimized for cylindrical surfaces.

Interestingly, Kif13A – a kinesin motor that directly binds Rab11 – is most enriched at the tips of membrane tubules (Delevoye et al., 2014). Moreover, Kif13A localizes to distinct Rab11-positive subdomains within sorting endosomes and is thought to initiate the formation of recycling endosomal tubules along microtubules through its motor activity (Delevoye et al., 2014). Interestingly, Nostrin directly interacts with the *Drosophila* Kif13A homologue Khc73 and colocalizes with Khc73-marked endosomes that move along microtubules. A close link between Nostrins and kinesin motors seem to be evolutionarily conserved and the interaction is likely mediated by a conserved bipartite tryptophan-based kinesin-1 binding motif (Dodding et al., 2011). Thus, in our model of cooperative recruitment, Cip4 stabilizes endosomal tubules, whereas Nostrin defines subdomains of recycling intermediates of endosomal tubules and makes contact with microtubules through the kinesin Khc-73 for long-range trafficking of recycling endosomes.

Nostrin and Cip4 regulate the epithelium morphogenesis of wing and thorax

A similar scenario might also take place during cell polarization of the wing epithelium. Here, Cip4 and Nostrin act together to control the polarized outgrowth of a single actin-rich protrusion called prehair, a process that also requires tight coupling of membrane trafficking and the cytoskeleton. The restriction of wing hair formation at the most distal apical vertex of each wing cell depends on the Frizzled–PCP signaling pathway. A key step in the cell polarization is the asymmetric localization of core PCP proteins at adjacent cell membranes within the plane of the epithelium. Thus, one of the central questions in understanding PCP signaling is how this asymmetric localization is achieved. Based on live-imaging studies, selective endocytosis and directional transport of Frizzled along polarized non-centrosomal microtubules have been proposed as possible mechanisms for asymmetric polarization (Harumoto et al., 2010; Shimada et al., 2006). Previous studies that had used microtubule antagonists already revealed an important role of the microtubule cytoskeleton in order to localize prehair initiation to the cell (Turner and Adler, 1995; Turner and Adler, 1998). Disruption of the microtubule cytoskeleton resulted in the development of multiple prehairs along the apical cell periphery (Turner and Adler, 1995). Multiple pre-hair formation is also caused by overexpression of Frizzled, presumably through an ectopic activation of the pre-hair nucleation machinery (Krasnow and Adler, 1994). However, the multiple wing hair phenotype in *nost;;cip4* double mutant wings does not seem to affect the asymmetric distribution of Frizzled. Interestingly, a similar Frizzled-independent multiple wing hair phenotype has recently been observed in mutants that affect casein kinase 1γ (CK1γ, also known as CSNK1G) (Gault et al., 2012). Loss of CK1γ disrupts the apical localization of Rab11 at the base of prehairs, suggesting that Ck1γ regulates Rab11-mediated polarized vesicle trafficking that is required for prehair nucleation (Gault et al., 2012). Consistently, expression of either a dominant-negative or a dominant-active Rab11 variant strongly induces the

Journal of Cell Science (2015) 128, 499–515 doi:10.1242/jcs.155929

formation of multiple wing hairs (Adler et al., 2013; Gault et al., 2012). Overexpression of Cip4 or Nostrin alone also phenocopies the multiple wing hair defect of *nost;;cip4* double mutants (Yan et al., 2013). Like CK1γ and Rab11, Cip4 and Nostrin accumulate at the base of forming prehairs. Because Nostrin colocalizes with Rab11-positive vesicles that move along microtubules, we propose that Nostrin is involved in Rab11-mediated polarized vesicle trafficking in the developing wing.

Polarized Rab11-dependent vesicle trafficking of E-cadherin is also needed for the hexagonal packing of wing cells. During this process, irregularly shaped cells adopt a hexagonal geometry by coordinated endocytosis and Rab11-dependent recycling of junctional E-cadherin. Hexagonal packing starts shortly after pupal molt and ends just before wing hair formation but, remarkably, also depends on components of the PCP pathway (Classen et al., 2005). The underlying molecular mechanism that links hexagonal packing and hair formation in the wing is unknown. However, both processes depend on vesicle trafficking because suppression of Rab11, Rab23 or the simultaneous knockdown of *cip4* and *nostrin* results not only in multiple wing hairs but also affects the regular hexagonal array of wing epithelial cells (Adler et al., 2013; Gault et al., 2012). A similar E-cadherin-dependent process of cell packing and remodeling can also be observed in the dorsal thorax, an epithelium that originally derived from the fused proximal parts of two wing imaginal discs. A role in E-cadherin membrane turnover has already been reported for Cip4 in the developing thorax epithelium of *Drosophila* (Leibfried et al., 2008). In cells that express *cip4* dsRNA, E-cadherin–GFP accumulates in apical punctate structures and elongated malformed tubules form at the cell cortex (Leibfried et al., 2008). These long and defective endocytic structures do not tolerate fixation and could only be observed in live-imaging experiments. In this study, we observed an even stronger defect on E-cadherin membrane dynamics upon simultaneous downregulation of Cip4 and Nostrin. The number of elongated malformed tubules that form at the cell cortex is clearly increased. Moreover, knockdown of both *cip4* and *nostrin* cause obvious defects in the formation of E-cadherin junctions, a phenotype that was never observed when suppressing either *cip4* or *nostrin*. These strong junctional defects might be responsible for the lethality of late pupae following RNAi transgene expression by the *aptereous*-Gal4 driver (data not shown). Thus, we conclude that both F-BAR proteins play an important cooperative rather than a redundant function in E-cadherin trafficking and junction maintenance.

MATERIALS AND METHODS

Cell culture, cell transfection and immunofluorescene microscopy

Drosophila S2R+ cells were cultured and transfected as described previously (Lammel et al., 2014). For spinning disk confocal microscopy, cells were re-plated on chambered cover glass (Lab-Tek) that had not been treated or had been pre-treated with concavalin A (Sigma).

Fly genetics

All crosses were performed at 25℃ unless otherwise indicated. *nostrin* mutant flies were generated using FRT-mediated recombination as described previously (Parks et al., 2004), by using the P-element insertions P{XP}d08142 and P{WH}f06363 (Bloomington stock center). The heat-shock *head involution defective* (*hs-hid*; Bloomington stock center) conditional lethal chromosome was used to obtain increased numbers of *nost;;cip4* double mutant flies. Flies were heat shocked for 2 h at 37℃ at day five and six. Transgenic flies were generated using phi-C31-mediated transgenesis targeted into the M{3xP3-RFP.attP}ZH-86F landing site (Bischof et al., 2007). RNAi lines were obtained from the VDRC and NIG stock center. Transgenic UAS-Nostrin–EGFP flies were generated following standard procedures.

Purification of recombinant Nostrin and antibody production

Rabbit anti-Nostrin antibodies were generated against a recombinant GST-tagged full-length short Nostrin isoform L protein (compare Fig. 1D) containing all coding exons (1S, 2, 3, 4, 5 and 6). GST–Nostrin fusion protein was expressed in *E. coli* (BL21) and purified with glutathione resin (GE Healthcare) under native conditions using Äkta FPLC (GE Healthcare). Animals were immunized with purified protein by Davids Biotechnologie (Germany). Affinity-purification was done as described previously (Qualmann et al., 1999).

Fixation and antibody staining of ovaries and/or egg chambers

Ovaries were dissected in ice-cold PBS and fixed in 4% paraformaldehyde/PBS for 15 min. Immunohistochemistry was performed as described previously (Bogdan et al., 2005). The following fluorescent markers were used: phalloidin tagged to Alexa-Fluor-488, Alexa-Fluor-568 and Alexa-Fluor-647 (all used at 1:100; Invitrogen). All antibodies were obtained from DSHB and were: anti-FasIII 1:20 (follicle cells), anti-Armadillo (N27A1) 1:30, DCAD2 (anti-E-cadherin) 1:20, anti-hts RC (ring canals) 1:20, anti–orb (oocyte) 1:50. DAPI was used at a dilution 1:1000. The polyclonal mouse anti-Cip4 antibody (A912; Antibody Core, UT Southwestern, Dallas) was used 1:100. The affinity-purified anti-Nostrin antibody (rabbit) was used 1:100. Affinity-purification of anti-Nostrin serum (generated against the full-length protein) was done as described previously (Qualmann et al., 1999). Secondary antibodies: goat anti-mouse Alexa-Fluor-488, Alexa-Fluor-568, Alexa-Fluor-647 and goat anti-rat Alexa-Fluor-568 (1:1000) (Molecular Probes). To quantify the localization defects of E-cadherin, an average intensitiy of E-cadherin was measured at the border between germline and follicle cells, and more basal in the center of follicle cells; the selected area of measurement is indicated in Fig. 6B (3 µm×11 µm rectangle). All images were acquired using identical microscope settings.

Cell culture, cell transfection, immunostaining and cloning

Drosophila S2R+ cells were propagated in 1×Schneider's *Drosophila* medium as described previously (Fricke et al., 2009). S2R+ cells were transfected as described previously (Lammel et al., 2014). Reverse transcriptase (RT)-PCR was performed with embryonic RNA as template to amplify the full-length Nostrin cDNA (short isoform). cDNA was subcloned into Gateway Entry Vectors (pENTR D-TOPO, Invitrogen) according to the manufacturer's instructions (*Escherichia coli* Expression System with Gateway Technology, Invitrogen). Inserts were sequenced and cloned into corresponding destination vectors (Drosophila Genomics Resource Center) by LR *in vitro* recombination, containing UASt promoters and N-terminal EGFP. The pQE-His-Tag system (Qiagen) was used to express fusion proteins for the immunization of rabbits.

Protein- and liposome-binding assays, and EM analyses of liposomes

Protein- and liposome-binding assays using Folch fraction type I lipids were conducted as described previously (Schneider et al., 2014). Liposome reconstitutions with purified lipids and protein- and liposome-binding assays were carried out as described previously (Dharmalingam et al., 2009). Cryo-transmission electron microscopy of Cip4- and Nostrin-coated liposomes was done on perforated carbon-film-covered copper grids (Quantifoil R3.5/1 Micro Tools GmbH, Jena, Germany). Samples that had had been frozen in liquid ethane-(~−180℃) were transferred to a pre-cooled cryo-transmission electron microscope operated at 120 kV (Philips CM 120; Eindhoven, The Netherlands) by using a cryo-transfer unit (Gatan 626-DH). Images were recorded with a 1k CCD Camera (FastScan F114, TVIPS, Gauting, Germany).

Freeze-fracturing of liposomes incubated with proteins (1.7 µM) was done according to Beetz et al., 2013. Immunolabeling of freeze-fracture replica was adapted from procedures we have recently developed in order to visualize proteins of the syndapin F-BAR-domain protein subfamily at

freeze-fractured membranes of cells and brain tissues (Koch et al., 2012a; Schneider et al., 2014), by using rabbit anti-GST antibodies (Qualmann et al., 1999; 1:100) and 10 nm gold-conjugated goat anti-rabbit IgGs (British Biocell International; 1:50) in single-labeling experiments.

For reconstitution experiments with both proteins, Nostrin was used as GST–Nostrin (1.7 µM) and CIP4 was liberated from its GST-tag using 1 U/100 µg GST-protein prescission protease (Amersham) during dialysis in 300 mM NaCl; 50 mM Na_3PO_4 pH 7.4 for 4 h at 4℃. Free GST was removed with glutathione-matrix (Genescript). The flow-through was concentrated afterwards with Amicon Ultra centrifugal filters and used for lipid floatation assays and for liposome binding studies (0.1 µM CIP4) subjected to EM analyses. In double-labeling experiments of freeze-fractured samples, rabbit anti-CIP4 antibodies (Fricke et al., 2009) detected by 10 nm gold-conjugated goat anti-rabbit antibodies (BBI International) were used in combination with guinea pig anti-GST antibodies (Kessels and Qualmann, 2002) and 15 nm gold-conjugated goat anti-guinea pig antibodies (BBI International) to visualize GST–Nostrin.

Samples were viewed using an EM 902A transmission electron microscope run at 80 kV (Zeiss, Oberkochen, Germany). Images were recorded digitally using a 1k FastScan-CCD-camera (TVIPS camera and software, Munich, Germany).

GST pull-down assays and co-immunoprecipitation experiments

An excess of GST–Cip4 fusion protein was immobilized on glutathione resin according to the manufacturer's instructions (GE Healthcare). About 10^8 S2R+ cells were harvested and lysed in 2 ml ice-cold lysis buffer (1×PBS, 1% NP40, 1 mM DTT and 1 mM PMSF). Lysates were centrifuged for 10 min at 10,000×***g*** (4℃) and 500 µl of the cytoplasmic supernatant were added to 30 µl of loaded glutathione resin. After incubation for 1 h at room temperature, unbound protein was washed away using four times 1 ml lysis buffer (room temperature). 10% of the preparation was used per lane on standard SDS-PAGE and analyzed by western blot analyses. Co-immunoprecipitation experiments were done with an anti-Khc73 antibody (Huckaba et al., 2011) as described previously (Fricke et al., 2009).

Structured illumination microscopy (SIM) imaging

SIM images were taken with an ELYRA S.1 Microscope (CellObserver SD, 63×/1.4 oil-immersion objective; Zeiss) with the software Zen 2010 D (Zeiss). Image acquisition was performed as described previously (Zobel and Bogdan, 2013). S2R+ cells were transferred on a glass coverslip and cells were incubated for 1 hour at 25℃. Cell fixation and phalloidin staining were done as described previously (Zobel and Bogdan, 2013).

In vivo spinning disk microscopy

Live imaging of S2R+ cells and E-cadherin–EGFP in dorsal thorax epithelium of 17 APF pupae were performed with a CellObserver s.d. spinning disk microscope (Zeiss) as reported recently (Sander et al., 2013). Cells were imaged through a 63×Plan-Apochromat (NA 1.4) oil-immersion objective using an inverted Zeiss Axio Observer.Z1 microscope with a CCD camera (Axiocam MRm camera, 6.45 µm×6.45 µm) and the laser lines 488 nm and 568 nm. For the imaging of living pupae we used only 25% laser intensity of the 488 nm Argon laser to avoid photodamage. Live imaging for E-cadherin–EGFP was acquired in wild type and mutant tissue using identical microscope settings and movies were scored blindly for malformed tubular membrane structures.

Acknowledgements

We thank Jörg Schultz for the phylogentic analysis of Nostrins, Manfred Frasch for sharing unpublished data on *nostrin* function during muscle development; Michael Way for sharing unpublished data on the conserved interaction between kinesin and Nostrin in mammals. We thank Thomas Huckaba and Athar Chishti for providing Khc37 plasmids and anti-Khc73 antibody. Veit Riechmann, Christian Klämbt and Meike Bechtold for helpful discussions and critical reading of the manuscript. We thank Fabian Bangel for help during initial split-YFP experiments, Elavarasi Dharmalingam for initial observations during Cip4/liposome assays, Frank Steiniger and Martin Westermann for help with the EM experiments. We thank the Bloomington Stock Center, VDRC, NIG-Fly for fly stocks.

Competing interests

The authors declare no competing or financial interests.

Author contributions

S.B. oversaw the initial biochemical, genetic and cell biological work, and also performed live-imaging experiments on E-cadherin localization. T.Z. generated the *nostrin-mutant* flies, performed the functional analysis of single- and double-mutant flies. K.B. cloned Khc-73 constructs, characterized the interaction between Nostrin and Khc-73, purified the anti-Nostrin antibody, and analyzed the expression of endogenous Nostrin and E-cadherin localization. N.K., K.S. and E.S. purified recombinant Cip4 and Nostrin proteins, performed the protein- and liposome-binding assays, and the EM analyses of liposomes. A.F. maintained insect cell culture and performed the cell transfection experiments. M.M.K. and B.Q. oversaw the liposome-binding assays and the EM analyses. S.B. wrote the manuscript with assistance from all authors.

Funding

This work was supported by grants from the Deutsche Forschungsgemeinschaft to M.M.K. (KE685/3-1 and 4-2), B.Q. (QU116/5-2 and 6-1) and S.B. (SFB 629, A13) and Cells-in-Motion Cluster of Excellence (EXC 1003 – CiM), University of Münster from the cluster of excellence ''Cells in Motion'' (CIM) to S.B. E.S. is funded by an IZKF grant to M.M.K. from the FSU Jena.

Supplementary material

Supplementary material available online at
http://jcs.biologists.org/lookup/suppl/doi:10.1242/jcs.155929/-/DC1

References

Adler, P. N. (2012). Chapter one – the frizzled/stan pathway and planar cell polarity in the Drosophila wing. In *Current Topics in Developmental Biology* (ed. Y. Yang), pp. 1-31. San Diego, CA: Academic Press.

Adler, P. N., Sobala, L. F., Thom, D. and Nagaraj, R. (2013). dusky-like is required to maintain the integrity and planar cell polarity of hairs during the development of the Drosophila wing. *Dev. Biol.* **379**, 76-91.

Ahmed, S., Bu, W., Lee, R. T. C., Maurer-Stroh, S. and Goh, W. I. (2010). F-BAR domain proteins: families and function. *Commun. Integr. Biol.* **3**, 116-121.

Aspenström, P. (2008). Roles of F-BAR/PCH proteins in the regulation of membrane dynamics and actin reorganization. *Int. Rev. Cell Mol. Biol.* **272**, 1-31.

Beetz, C., Koch, N., Khundadze, M., Zimmer, G., Nietzsche, S., Hertel, N., Huebner, A. K., Mumtaz, R., Schweizer, M., Dirren, E. et al. (2013). A spastic paraplegia mouse model reveals REEP1-dependent ER shaping. *J. Clin. Invest.* **123**, 4273-4282.

Bischof, J., Maeda, R. K., Hediger, M., Karch, F. and Basler, K. (2007). An optimized transgenesis system for Drosophila using germ-line-specific phiC31 integrases. *Proc. Natl. Acad. Sci. USA* **104**, 3312-3317.

Bogard, N., Lan, L., Xu, J. and Cohen, R. S. (2007). Rab11 maintains connections between germline stem cells and niche cells in the Drosophila ovary. *Development* **134**, 3413-3418.

Bogdan, S., Stephan, R., Löbke, C., Mertens, A. and Klämbt, C. (2005). Abi activates WASP to promote sensory organ development. *Nat. Cell Biol.* **7**, 977-984.

Bu, W., Lim, K. B., Yu, Y. H., Chou, A. M., Sudhaharan, T. and Ahmed, S. (2010). Cdc42 interaction with N-WASP and Toca-1 regulates membrane tubulation, vesicle formation and vesicle motility: implications for endocytosis. *PLoS ONE* **5**, e12153.

Chen, Y., Aardema, J., Kale, S., Whichard, Z. L., Awomolo, A., Blanchard, E., Chang, B., Myers, D. R., Ju, L., Tran, R. et al. (2013). Loss of the F-BAR protein CIP4 reduces platelet production by impairing membrane-cytoskeleton remodeling. *Blood* **122**, 1695-1706.

Classen, A.-K., Anderson, K. I., Marois, E. and Eaton, S. (2005). Hexagonal packing of Drosophila wing epithelial cells by the planar cell polarity pathway. *Dev. Cell* **9**, 805-817.

Delevoye, C., Miserey-Lenkei, S., Montagnac, G., Gilles-Marsens, F., Paul-Gilloteaux, P., Giordano, F., Waharte, F., Marks, M. S., Goud, B. and Raposo, G. (2014). Recycling endosome tubule morphogenesis from sorting endosomes requires the kinesin motor KIF13A. *Cell Reports* **6**, 445-454.

Demeter, J. and Sazer, S. (1998). imp2, a new component of the actin ring in the fission yeast Schizosaccharomyces pombe. *J. Cell Biol.* **143**, 415-427.

Dharmalingam, E., Haeckel, A., Pinyol, R., Schwintzer, L., Koch, D., Kessels, M. M. and Qualmann, B. (2009). F-BAR proteins of the syndapin family shape the plasma membrane and are crucial for neuromorphogenesis. *J. Neurosci.* **29**, 13315-13327.

Dodding, M. P., Mitter, R., Humphries, A. C. and Way, M. (2011). A kinesin-1 binding motif in vaccinia virus that is widespread throughout the human genome. *Embo J.* **30**, 4523-4538.

Doyle, K., Hogan, J., Lester, M. and Collier, S. (2008). The Frizzled Planar Cell Polarity signaling pathway controls Drosophila wing topography. *Dev. Biol.* **317**, 354-367.

Fankhauser, C., Reymond, A., Cerutti, L., Utzig, S., Hofmann, K. and Simanis, V. (1995). The S. pombe cdc15 gene is a key element in the reorganization of F-actin at mitosis. *Cell* **82**, 435-444.

Feng, Y., Hartig, S. M., Bechill, J. E., Blanchard, E. G., Caudell, E. and Corey, S. J. (2010). The Cdc42-interacting protein-4 (CIP4) gene knock-out mouse reveals delayed and decreased endocytosis. *J. Biol. Chem.* **285**, 4348-4354.
Fricke, R., Gohl, C., Dharmalingam, E., Grevelhörster, A., Zahedi, B., Harden, N., Kessels, M., Qualmann, B. and Bogdan, S. (2009). Drosophila Cip4/Toca-1 integrates membrane trafficking and actin dynamics through WASP and SCAR/WAVE. *Curr. Biol.* **19**, 1429-1437.
Fricke, R., Gohl, C. and Bogdan, S. (2010). The F-BAR protein family Actin' on the membrane. *Commun. Integr. Biol.* **3**, 89-94.
Frost, A., Perera, R., Roux, A., Spasov, K., Destaing, O., Egelman, E. H., De Camilli, P. and Unger, V. M. (2008). Structural basis of membrane invagination by F-BAR domains. *Cell* **132**, 807-817.
Frost, A., Unger, V. M. and De Camilli, P. (2009). The BAR domain superfamily: membrane-molding macromolecules. *Cell* **137**, 191-196.
Fütterer, K. and Machesky, L. M. (2007). ''Wunder'' F-BAR domains: going from pits to vesicles. *Cell* **129**, 655-657.
Gault, W. J., Olguin, P., Weber, U. and Mlodzik, M. (2012). Drosophila CK1-γ, gilgamesh, controls PCP-mediated morphogenesis through regulation of vesicle trafficking. *J. Cell Biol.* **196**, 605-621.
Gelbart, W. M. and Emmert, D. B. (2013). *FlyBase High Throughput Expression Pattern Data*. FBrf0221009.
Godt, D. and Tepass, U. (1998). Drosophila oocyte localization is mediated by differential cadherin-based adhesion. *Nature* **395**, 387-391.
Gohl, C., Banovic, D., Grevelhörster, A. and Bogdan, S. (2010). WAVE forms hetero- and homo-oligomeric complexes at integrin junctions in Drosophila visualized by bimolecular fluorescence complementation. *J. Biol. Chem.* **285**, 40171-40179.
Golic, K. G. and Lindquist, S. (1989). The FLP recombinase of yeast catalyzes site-specific recombination in the Drosophila genome. *Cell* **59**, 499-509.
González-Reyes, A. and St Johnston, D. (1998). Patterning of the follicle cell epithelium along the anterior-posterior axis during Drosophila oogenesis. *Development* **125**, 2837-2846.
Grammont, M. and Irvine, K. D. (2001). fringe and Notch specify polar cell fate during Drosophila oogenesis. *Development* **128**, 2243-2253.
Harumoto, T., Ito, M., Shimada, Y., Kobayashi, T. J., Ueda, H. R., Lu, B. and Uemura, T. (2010). Atypical cadherins Dachsous and Fat control dynamics of noncentrosomal microtubules in planar cell polarity. *Dev. Cell* **19**, 389-401.
Heath, R. J. W. and Insall, R. H. (2008). F-BAR domains: multifunctional regulators of membrane curvature. *J. Cell Sci.* **121**, 1951-1954.
Henne, W. M., Boucrot, E., Meinecke, M., Evergren, E., Vallis, Y., Mittal, R. and McMahon, H. T. (2010). FCHo proteins are nucleators of clathrin-mediated endocytosis. *Science* **328**, 1281-1284.
Ho, H.-Y. H., Rohatgi, R., Lebensohn, A. M., Le Ma,, Li, J, Gygi, S. P and Kirschner, M. W. (2004). Toca-1 mediates Cdc42-dependent actin nucleation by activating the N-WASP-WIP complex. *Cell* **118**, 203-216.
Horne-Badovinac, S. and Bilder, D. (2005). Mass transit: epithelial morphogenesis in the Drosophila egg chamber. *Dev. Dyn.* **232**, 559-574.
Huckaba, T. M., Gennerich, A., Wilhelm, J. E., Chishti, A. H. and Vale, R. D. (2011). Kinesin-73 is a processive motor that localizes to Rab5-containing organelles. *J. Biol. Chem.* **286**, 7457-7467.
Icking, A., Matt, S., Opitz, N., Wiesenthal, A., Müller-Esterl, W. and Schilling, K. (2005). NOSTRIN functions as a homotrimeric adaptor protein facilitating internalization of eNOS. *J. Cell Sci.* **118**, 5059-5069.
Itoh, T. and De Camilli, P. (2006). BAR, F-BAR (EFC) and ENTH/ANTH domains in the regulation of membrane–cytosol interfaces and membrane curvature. *Biochim. Biophys. Acta* **1761**, 897-912.
Kessels, M. M. and Qualmann, B. (2002). Syndapins integrate N-WASP in receptor-mediated endocytosis. *EMBO J.* **21**, 6083-6094.
Koch, D., Westermann, M., Kessels, M. M. and Qualmann, B. (2012a). Ultrastructural freeze-fracture immunolabeling identifies plasma membrane-localized syndapin II as a crucial factor in shaping caveolae. *Histochem. Cell Biol.* **138**, 215-230.
Koch, N., Dharmalingam, E., Westermann, M., Qualmann, B., Thomas, U. and Kessels, M. M. (2012b). Abp1 utilizes the Arp2/3 complex activator Scar/WAVE in bristle development. *J. Cell Sci.* **125**, 3578-3589.
Kovacevic, I., Hu, J., Siehoff-Icking, A., Opitz, N., Griffin, A., Perkins, A. C., Munn, A. L., Müller-Esterl, W., Popp, R., Fleming, I. et al. (2012). The F-BAR protein NOSTRIN participates in FGF signal transduction and vascular development. *EMBO J.* **31**, 3309-3322.
Krasnow, R. E. and Adler, P. N. (1994). A single frizzled protein has a dual function in tissue polarity. *Development* **120**, 1883-1893.
Lammel, U., Bechtold, M., Risse, B., Berh, D., Fleige, A., Bunse, I., Jiang, X., Klämbt, C. and Bogdan, S. (2014). The Drosophila FHOD1-like formin Knittrig acts through Rok to promote stress fiber formation and directed macrophage migration during the cellular immune response. *Development* **141**, 1366-1380.
Leibfried, A., Fricke, R., Morgan, M. J., Bogdan, S. and Bellaiche, Y. (2008). Drosophila Cip4 and WASp define a branch of the Cdc42-Par6-aPKC pathway regulating E-cadherin endocytosis. *Curr. Biol.* **18**, 1639-1648.
López-Schier, H. and St Johnston, D. (2001). Delta signaling from the germ line controls the proliferation and differentiation of the somatic follicle cells during Drosophila oogenesis. *Genes Dev.* **15**, 1393-1405.
Lupas, A. (1996). Prediction and analysis of coiled-coil structures. *Methods Enzymol.* **266**, 513-525.
McCaffrey, R., St Johnston, D. and González-Reyes, A. (2006). A novel mutant phenotype implicates dicephalic in cyst formation in the Drosophila ovary. *Dev. Dyn.* **235**, 908-917.
McMahon, H. T. and Gallop, J. L. (2005). Membrane curvature and mechanisms of dynamic cell membrane remodelling. *Nature* **438**, 590-596.
Nahm, M., Long, A. A., Paik, S. K., Kim, S., Bae, Y. C., Broadie, K. and Lee, S. (2010). The Cdc42-selective GAP rich regulates postsynaptic development and retrograde BMP transsynaptic signaling. *J. Cell Biol.* **191**, 661-675.
Parks, A. L., Cook, K. R., Belvin, M., Dompe, N. A., Fawcett, R., Huppert, K., Tan, L. R., Winter, C. G., Bogart, K. P., Deal, J. E. et al. (2004). Systematic generation of high-resolution deletion coverage of the Drosophila melanogaster genome. *Nat. Genet.* **36**, 288-292.
Qualmann, B., Roos, J., DiGregorio, P. J. and Kelly, R. B. (1999). Syndapin I, a synaptic dynamin-binding protein that associates with the neural Wiskott-Aldrich syndrome protein. *Mol. Biol. Cell* **10**, 501-513.
Qualmann, B., Koch, D. and Kessels, M. M. (2011). Let's go bananas: revisiting the endocytic BAR code. *EMBO J.* **30**, 3501-3515.
Roberts-Galbraith, R. H., Chen, J.-S., Wang, J. and Gould, K. L. (2009). The SH3 domains of two PCH family members cooperate in assembly of the Schizosaccharomyces pombe contractile ring. *J. Cell Biol.* **184**, 113-127.
Robinson, D. N. and Cooley, L. (1997). Genetic analysis of the actin cytoskeleton in the Drosophila ovary. *Annu. Rev. Cell Dev. Biol.* **13**, 147-170.
Sander, M., Squarr, A. J., Risse, B., Jiang, X. and Bogdan, S. (2013). Drosophila pupal macrophages – a versatile tool for combined ex vivo and in vivo imaging of actin dynamics at high resolution. *Eur. J. Cell Biol.* **92**, 349-354.
Sato, K., Nishida, K. M., Shibuya, A., Siomi, M. C. and Siomi, H. (2011). Maelstrom coordinates microtubule organization during Drosophila oogenesis through interaction with components of the MTOC. *Genes Dev.* **25**, 2361-2373.
Schneider, K., Seemann, E., Liebmann, L., Ahuja, R., Koch, D., Westermann, M., Hübner, C. A., Kessels, M. M. and Qualmann, B. (2014). ProSAP1 and membrane nanodomain-associated syndapin I promote postsynapse formation and function. *J. Cell Biol.* **205**, 197-215.
Shimada, Y., Yonemura, S., Ohkura, H., Strutt, D. and Uemura, T. (2006). Polarized transport of Frizzled along the planar microtubule arrays in Drosophila wing epithelium. *Dev. Cell* **10**, 209-222.
Shimada, A., Niwa, H., Tsujita, K., Suetsugu, S., Nitta, K., Hanawa-Suetsugu, K., Akasaka, R., Nishino, Y., Toyama, M., Chen, L. et al. (2007). Curved EFC/F-BAR-domain dimers are joined end to end into a filament for membrane invagination in endocytosis. *Cell* **129**, 761-772.
Strutt, D. I. (2002). The asymmetric subcellular localisation of components of the planar polarity pathway. *Semin. Cell Dev. Biol.* **13**, 225-231.
Suetsugu, S. (2010). The proposed functions of membrane curvatures mediated by the BAR domain superfamily proteins. *J. Biochem.* **148**, 1-12.
Suetsugu, S. and Gautreau, A. (2012). Synergistic BAR-NPF interactions in actin-driven membrane remodeling. *Trends Cell Biol.* **22**, 141-150.
Tanentzapf, G., Smith, C., McGlade, J. and Tepass, U. (2000). Apical, lateral, and basal polarization cues contribute to the development of the follicular epithelium during Drosophila oogenesis. *J. Cell Biol.* **151**, 891-904.
Theiss, C., Neuhaus, A., Schliebs, W. and Erdmann, R. (2012). TubStain: a universal peptide-tool to label microtubules. *Histochem. Cell Biol.* **138**, 531-540.
Tsujita, K., Suetsugu, S., Sasaki, N., Furutani, M., Oikawa, T. and Takenawa, T. (2006). Coordination between the actin cytoskeleton and membrane deformation by a novel membrane tubulation domain of PCH proteins is involved in endocytosis. *J. Cell Biol.* **172**, 269-279.
Turner, C. M. and Adler, P. N. (1995). Morphogenesis of Drosophila pupal wings in vitro. *Mech. Dev.* **52**, 247-255.
Turner, C. M. and Adler, P. N. (1998). Distinct roles for the actin and microtubule cytoskeletons in the morphogenesis of epidermal hairs during wing development in Drosophila. *Mech. Dev.* **70**, 181-192.
Vachias, C., Couderc, J.-L. and Grammont, M. (2010). A two-step Notch-dependant mechanism controls the selection of the polar cell pair in Drosophila oogenesis. *Development* **137**, 2703-2711.
Xu, J., Lan, L., Bogard, N., Mattione, C. and Cohen, R. S. (2011). Rab11 is required for epithelial cell viability, terminal differentiation, and suppression of tumor-like growth in the Drosophila egg chamber. *PLoS ONE* **6**, e20180.
Yan, S., Lv, Z., Winterhoff, M., Wenzl, C., Zobel, T., Faix, J., Bogdan, S. and Grosshans, J. (2013). The F-BAR protein Cip4/Toca-1 antagonizes the formin Diaphanous in membrane stabilization and compartmentalization. *J. Cell Sci.* **126**, 1796-1805.
Zimmermann, K., Opitz, N., Dedio, J., Renne, C., Muller-Esterl, W. and Oess, S. (2002). NOSTRIN: a protein modulating nitric oxide release and subcellular distribution of endothelial nitric oxide synthase. *Proc. Natl. Acad. Sci. USA* **99**, 17167-17172.
Zobel, T. and Bogdan, S. (2013). A high resolution view of the fly actin cytoskeleton lacking a functional WAVE complex. *J. Microsc.* **251**, 224-231.